Research Article

TRANSPARENT PROCESS OPEN ACCESS Life Science Alliance

Mutual feedback regulation between Poly(A)-specific ribonuclease (PARN) and cognate microRNAs

Athanasios Kyritsis[1], Rafailia AA Beta[1,*], Diana Scutelnic[1,*], Vasiliki Stravokefalou[1], Valerio Del Vescovo[2], Zoi V Arsenopoulou[1], Konstantinos Papikinos[1,2], Margherita Grasso[2], Francesca Fontana[2], Paraskevi Moutopoulou[1], Alexandros Tsiporis[1], Martina Samiotaki[3], George Panayotou[3], Michela A Denti[2], Nikolaos AA Balatsos[1]

The majority of pri-miRNAs acquire a 5′ cap and 3′ poly(A) tail. Mature miRNAs recruit deadenylases that shorten poly(A) tails triggering target mRNA degradation. Poly(A)-specific ribonuclease (PARN) is a deadenylase that also mediates late steps of noncoding RNA maturation. Herein, we show that PARN affects the expression of a subset of miRNAs in NCI-H520 cells of lung cancer origin, including miR-29a and miR-1207, which are also predicted to target PARN mRNA. PARN associates with pri-miR-29a and pri-miR-1207 regulating their poly(A) lengths. Conversely, miR-29a-3p and miR-1207-5p bind the 3′ UTR of PARN mRNA and regulate its expression. Cleavage and polyadenylation specificity factor 6 (CPSF6) recruits PARN to pri-miRNAs and together they affect primary and mature miR-29a-3p levels. Modulation of PARN, miR-29a-3p, or miR-1207-5p expression affects cell migration. We present a model to describe the dynamic relation between PARN and miR-29a and discuss its biological significance.

DOI 10.26508/lsa.202503341 | Received 4 April 2025 | Revised 16 February 2026 | Accepted 19 February 2026 | Published online 13 March 2026

Introduction

PARN is a well-characterized ribonuclease in vertebrates. Originally described as a 74-kD exoribonuclease that specifically degrades poly(A) tails, it is the only currently known deadenylase to interact directly with both the poly(A) tail and the m^7G-cap (Dehlin et al, 2000; Gao et al, 2000; Martinez et al, 2001) and competes with other cap-binding proteins that regulate its activity, such as the cap-binding complex (CBC) and the eukaryotic initiation factor 4E (eIF4E) (Seal et al, 2005; Balatsos et al, 2006). PARN is involved in the destabilization of mRNAs with AU-rich elements (Lai et al, 2003; Lin et al, 2007b), where RBPs, such as KSRP, tristetraprolin and CUGBP, may recruit PARN to destabilize various mRNAs, including cancer related transcripts such as c-jun, PLAU, c-fos, and TNF (Lai & Blackshear, 2001; Tran et al, 2003; Gherzi et al, 2004; Chou et al, 2006; Moraes et al, 2006; Suswam et al, 2008). Furthermore, PARN regulates the stability of TP53 mRNA through an ARE and an adjacent miR-504/miR125b-targeting site in the 3′ UTR (Zhang et al, 2015). PARN is involved in the biogenesis of noncoding RNAs, including snoRNAs, piRNAs, and 18S pre-rRNA (Berndt et al, 2012; Moon et al, 2015; Tang et al, 2016; Ishikawa et al, 2017; Montellese et al, 2017), as well as in the maturation of the telomerase RNA component (Moon et al, 2015; Shukla et al, 2016). The latter has significant clinical implications; loss-of-function mutations in PARN impair telomerase RNA component processing and stability, leading to reduced telomerase activity and accelerated telomere shortening, linking PARN to telomere-associated diseases including dyskeratosis congenita, Hoyeraal–Hreidarsson syndrome, bone-marrow failure and pulmonary fibrosis (Dhanraj et al, 2015; Moon et al, 2015; Stuart et al, 2015; Tummala et al, 2015). PARN trims selected miRNAs to complete their maturation (Lee et al, 2019), and it is involved in the destabilization and turnover of UG-rich microRNAs in the cytoplasm, including miR-21 and miR-122 (Boele et al, 2014; Katoh et al, 2015).

The canonical biogenesis pathway for the majority of miRNAs suggests that miRNA genes are transcribed by RNA polymerase II to generate primary transcripts (pri-miRNAs), which acquire 5′ cap and 3′ poly(A) tail (Ha & Kim, 2014; Kim et al, 2016). Then, the maturation of miRNAs is described by a two-step model where pri-miRNAs are processed to precursor miRNAs (pre-miRNAs) by the microprocessor complex in the nucleus and the released hairpin is exported to the cytoplasm, where it is further processed by DICER, producing a duplex RNA of ~22 nt (Gregory et al, 2004; Ha & Kim, 2014). Control of miRNA biogenesis may occur upstream the microprocessor. Alternatively, noncanonical, pathways for miRNA biogenesis downstream the microprocessor have been described,

[1]Department of Biochemistry and Biotechnology, University of Thessaly, Larissa, Greece [2]Department of Cellular, Computational and Integrative Biology - CIBIO, University of Trento, Trento, Italy [3]B.S.R.C. "Alexander Fleming", Vari, Greece

Correspondence: michela.denti@unitn.it; balatsos@bio.uth.gr
Valerio Del Vescovo's present address is Kapadi Italy SRL, Milano, Italy
Konstantinos Papikinos's present address is Imperial Brands PLC, Bristol, England
Margherita Grasso's present address is L.N.Age Srl, Roma, Italy
*Rafailia AA Beta and Diana Scutelnic contributed equally to this work

which bypass the main DROSHA or DICER steps of the canonical pathway, such as mirtrons (Okamura et al, 2007; Ruby et al, 2007), the m^7G-capped pre-miR-320 (Chong et al, 2010), as well as small RNAs generated by snoRNAs (Ender et al, 2008), tRNAs (Babiarz et al, 2008), and small nuclear RNA-like viral RNAs (Cazalla et al, 2011) which bypass DROSHA processing, whereas they are further processed by DICER cleavage. On the other hand, pri-miR-451 is a DROSHA substrate but bypasses DICER, where AGO2 generates pre-miR-451, which is further trimmed to appropriate length by PARN (Yoda et al, 2013).

Based on the fact that the majority of pri-miRNAs acquire cap and poly(A) tails and that PARN interacts with the cap to catalyze poly(A) shortening, we investigate the role of PARN on miRNA biogenesis and overall stability. We show that PARN regulates the expression of a specific subset of miRNAs, including miRNA-29a and miR-1207. PARN precipitates with pri-miR-29a and alters its poly(A) status and stability. We find that PARN interacts with Cleavage and Polyadenylation Specificity Factor 6, CPSF6, and both affect miR-29a-3p expression. These observations demonstrate that PARN mediates the early steps of maturation for a specific subset of microRNAs and highlights the role of CPSF6 to recruit PARN to the newly synthesized polyadenylated primary microRNA transcripts. On the other hand, miR-29a-3p and miR-1207-5p target the 3′ UTR of PARN mRNA, and reduce PARN mRNA and protein levels. To assess the potential biological significance of the previous and based on published works, we investigate PARN's role in cell migration and we find that it is impaired upon disturbing the expression of PARN and both microRNAs. Conclusively, this work highlights PARN as a guardian of miRNA biogenesis, whereas its dynamic relation with specific miRNAs reflects in processes related to cancer.

Results

PARN affects the expression levels of a subset of microRNAs

To investigate the role of PARN on miRNA expression, we silenced PARN in NCI-H520 cells (Fig 1A). The impact of PARN silencing on miRNA expression profile was examined by Agilent miRNA microarrays. 35 miRNAs were observed to be deregulated (−0.5 < log [PARN/MSH] > 0.5) upon PARN silencing: 23 up-regulated and 12 down-regulated (Fig 1B). We performed bioinformatic analyses to identify potential targets of the miRNAs deregulated upon PARN silencing. Of the deregulated miRs we focused on miR-29a-3p and miR1207-5p; the former is the second most up-regulated (almost six-fold) and the latter the least, whereas both of them are predicted to target the 3′ UTR of PARN mRNA itself (see below).

The up-regulation of miR-29a-3p and miR-1207-5p observed by the microarray analysis was validated by qRT-PCR. Silencing of PARN increased miR-29a-3p levels about 80% when compared with those of cells transfected with empty vector (Fig 1C, left panel), whereas an increase of ~60% was observed for miR-1207-5p (Fig 1C, right panel). Differences in fold-change magnitude between microarray and qRT-PCR are well documented and most likely reflect inherent methodological differences between the platforms rather than experimental error. These results show that PARN affect the overall expression of a specific subset of miRNAs.

PARN affects the stability of pri-miR-29a and miR-29a-3p

As the microarray results represent the sum total of pri-miRNA and pre-miRNA stability and processing, as well as reflect the stability of mature miRNAs (Bail et al, 2010), we examined the impact of PARN on the turnover rates of miR-29a-3p upon inhibition of transcription with Actinomycin D (ActD), keeping in mind that the latter is expected to affect the synthesis of pri-miRNAs and not subsequent processing events (Bail et al, 2010). We focused on miR-29, as it seems to be more affected by PARN (Fig 1) and, in turn, miR-29-3p is predicted to target PARN mRNA more efficiently (see Results section below and Fig 4). PARN was either silenced or overexpressed in NCI-H520 cells, where the cells were serum-starved to induce synchronization, recovered and treated with ActD over a time course of 12 h and the levels of pri-miR-29a and miR-29a-3p were analyzed by qRT-PCR (Fig 2A).

PARN silencing resulted in a reproducible accumulation of pri-miR-29a detectable 4 h post ActD treatment (Fig 2B, right panel). On the other hand, miR-29a-3p levels were modestly above control values at early time points, consistent with the microarray results. These levels subsequently declined and decreased below control values ~8 h post ActD addition (Fig 2B, right panel). Overall, PARN silencing modulated the relative levels of primary and mature miR-29a, with changes in mature miR-29a-3p remaining modest in magnitude (~8–12%), consistent with an effect on processing efficiency rather than large changes in steady-state abundance.

Following PARN overexpression, at the time of ActD addition (0 h) the levels of pri-miRs were higher compared with control ones (Fig 2B, left panel), they decreased below control levels within 1 h post ActD treatment and stabilized after ~4 h (Fig 2B, left panel).

Moreover, a catalytically inactive form of PARN (PARN E30A) (Ren et al, 2002) was overexpressed using the same conditions as PARN to examine whether deadenylase activity affects the overall levels of pri-miR-29a and miR-29a-3p. Indeed, the levels of pri-miR-29a remained relatively stable for 2 h and then gradually decreased, reaching values significantly below the control after 8 h of Act D treatment (Fig 2B, middle panel). On the other hand, miR-29a-3p levels showed a small increase but remained lower than the control values throughout the time course (Fig 2B, middle panel), whereas the rate of this increase was clearly lower than that observed upon PARN overexpression (compare Fig 2B, left and middle panels), (Fig 2C and D).

Together, these data indicate that altering PARN expression modulates the balance between primary and mature miR-29a, consistent with a role in fine-tuning pri-miRNA processing rather than inducing large changes in mature miRNA abundance.

PARN affects the length of the poly(A) tail of pri-miR-29a

Since primary microRNAs are RNA polymerase II trancripts and are polyadenylated, we reasoned that PARN might be involved in the maturation process of pri-miR-29a through its poly(A) tail. We transfected NCI-H520 cells either with specific shRNAs against

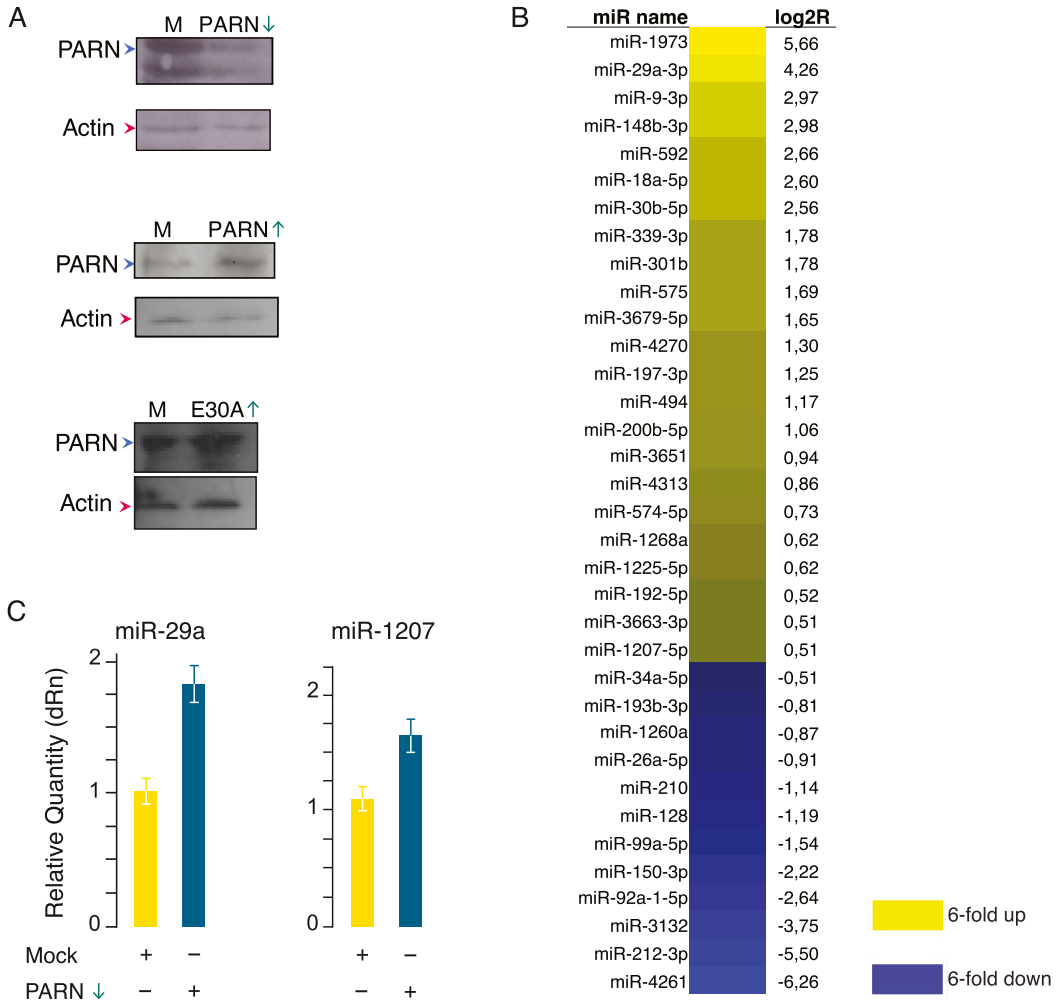

Figure 1. PARN affects the expression levels of a subset of microRNAs.
MicroRNA microarrays. **(A)** Western blots of the transfected cells used in this study after silencing PARN (upper panel), up-regulating PARN (middle panel) and up-regulating a catalytically inactive PARN E30A (lower panel). Actin served as a loading control. Positions of PARN and actin are denoted with blue and red arrowheads, respectively. Upward (↑) and downward (↓) arrows denote PARN up-regulation and silencing, respectively. **(B)** Heat map of microRNA microarray analysis upon silencing of PARN in NCI-H520 cells. Numbers on the right of the map indicate $\log_2$ fold-change relative to control cells. **(C)** Effect of PARN on miR-29a-3p and miR-1207-5p levels. Transfections were performed for 72 h. Cells were transfected with empty vector (mock) and specific constructs to silence PARN.

PARN or with empty vector as control (mock), and analyzed the poly(A) status of pri-miR-29a with LM-PAT assay (Salles et al, 1999). Accordingly, the PCR products were generated using specific primers (Fig 2D) to detect polyadenylated pri-miR-29a. The minimal expected non-polyadenylated product is ~380 nt-long, that is, between primer *α* and the 5′ end of the poly(A) tail. Such products are observed due to the priming from this position during reverse transcription (indicated by an arrowhead in Fig 2D). Apart from this product, additional bands corresponding to polyadenylated transcripts (~480 nt-long) are observed because of the saturation of the poly(A) with anchor primer (Salles et al, 1999). The analysis of the PCR products shows that when PARN is down-regulated, transcripts with varying poly(A) lengths longer than 500 nts accumulate (Fig 2D, lane 5, indicated as poly(A)). The minimal, as well as the 480-nt products were present in the control extracts (Fig 2D, lane 2), yet transcripts beyond this length could hardly be observed (Fig 2D, lanes 2 and 5). This can be attributed to the fact that when PARN is present the tails are rapidly degraded allowing further processing of the primary transcripts, whereas the impaired expression of the enzyme results to the accumulation of unprocessed polyadenylated pri-miR-29a transcripts.

To further validate these observations, we performed a RACE-PAT analysis of pri-miR-29a. Consistent with the LM-PAT results, PARN silencing led to accumulation of polyadenylated pri-miR-29a transcripts (Fig S1).

Together, these data indicate that PARN modulates the poly(A) status of pri-miR-29a and suggest a role for PARN in early steps of primary miRNA processing.

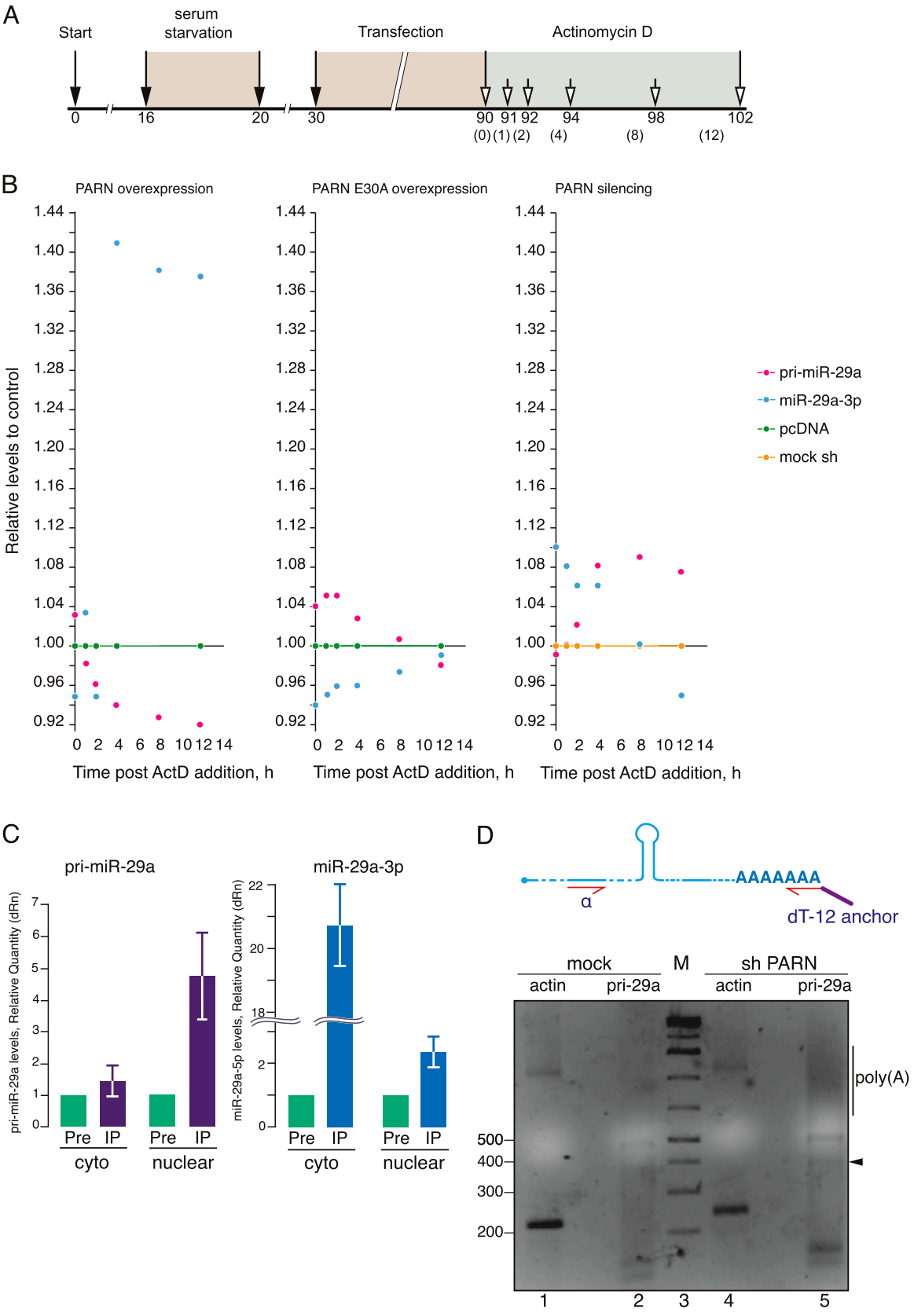

Figure 2. miR-29a turnover kinetics upon inhibition of transcription.
(A) Schematic of experimental design to measure cellular miRNA turnover kinetics. Cultured mammalian cells were serum-starved, allowed for recovery, transfected with appropriate plasmids and finally, treated with ActD. Total RNA samples collected in a time course experiment were analyzed by qRT-PCR. Numbers below the line

PARN interacts with pri-miR-29a and mature miR-29a-3p

We next wished to verify whether PARN interacts with pri-miR-29a or miR-29a-3p. We performed RNA immunoprecipitation in nuclear and cytoplasmic extracts from NCI-H520 cells with PARN and preimmune antisera. Analysis of the associated RNAs with qRT-PCR revealed that PARN precipitates with pri-miR-29a in nuclear extracts (fivefold increase compared with preimmune; Fig 3A), whereas this interaction in the cytoplasmic fraction was significantly lower (0.5-fold when compared with pre-immune) (Fig 3A). The profile was reversed for the mature miR-29a, where significantly higher levels of miR-29a-3p precipitated with PARN in the cytoplasm compared with those in the nucleus (Fig 3B). These results show that PARN interacts with primary forms of miR-29a-3p in the nucleus. In addition, RNA immunoprecipitation analysis revealed association of PARN with its own mRNA in the cytoplasm (Fig S2).

Overall, these findings show that PARN influences the stability and poly(A) status of pri-miR-29a and associates with both primary and mature miR-29a in the nucleus and in the cytoplasm, supporting a role for PARN in early steps of miR-29a maturation.

miR-29a-3p and miR-1207-5p interact with 3′ UTR of PARN mRNA and affect PARN levels

As mentioned above, bioinformatics analyses identified the 3′ UTR of PARN mRNA as a potential target of miR-29a-3p and miR-1207-5p. Both miRs were predicted to each target two sites in the 1,016 nt-long 3′ UTR of PARN mRNA (sites 1–4, Fig 3C). To validate these interactions, we cloned sequences of the 3′UTR of PARN mRNA downstream the firefly luciferase gene in pGLO vector and transfected HeLa cells. More specifically, the cloned sequences were the full 3′ UTR of PARN (pGLO-PARN), portions of the 3′UTR sequence containing one binding site for miR-29a-3p, one for miR-1207-5p or one for each miR (pGLO-PARN-A, pGLO-PARN-B, and pGLO-PARN-C, respectively; Fig 4D), sequences with each one of the miR-binding sites mutated (pGLO-PARN-D1–D4), or double mutations of both binding sites of miR-29-3p or miR-1207-5p (pGLO-PARN-D1/3 and pGLO-PARN-D2/4; Fig 4D). HeLa cells were transfected with plasmids to overexpress miR-29a-3p (Fig 3E) and the examination of the binding of miR-29a-3p to PARN 3′ UTR is shown in Fig 3F and G, as described (see the Materials and Methods section; Luciferase assay). Luciferase signal was reduced upon the expression of miR-29a-3p when both or each of its binding sites are present in the luciferase construct (Fig 3F). The binding to site 3 seems to be more efficient than site 1 (compare Fig 3F, bars pGLO-PARN-A and pGLO-PARN-C). Moreover, mutations and deletions within PARN 3′UTR constructs showed that each of the miRNAs binds to both its target sites independently (Fig 3G). Thus, miR-29a-3p hybridizes to the 3′UTR of PARN mRNA and sites 1 and 3 are binding sequences. Analogous results were obtained for miR-1207-5p; HeLa cells were transfected with plasmids to overexpress miR-1207-5p (Fig 3H) and the effect on the luciferase construct products are summarized in Fig 3I and J. The results showed that miR-1207 binds to the 3′UTR of PARN and predicted sites 2 and 4 are two such hybridization sequences. Both target sites are necessary for translational repression by each miRNA (Fig 3E and G). Overall, miR-29a-3p and miR-1207-5p bind to the 3′ UTR of PARN mRNA.

We next tested whether miR-29a-3p and miR-1207-5p regulate the levels of PARN protein in NCI-H520 cells. Upon miR-29a-3p overexpression, PARN mRNA and protein levels decreased; PARN mRNA was reduced to ~50% at 24 h and 30% at 48 h, when compared with cells transfected with empty pSiUx plasmid (Fig 4A). At the protein level, miR-29a-3p overexpression substantially reduced PARN when compared with control conditions, namely WT cells and cells transfected with empty vector (Fig 4B). miR-1207-5p overexpression showed minimal effect on PARN mRNA levels (Fig 4A), yet it efficiently decreased PARN protein levels upon 48 and 72 h post transfection (Fig 4B, compare lanes 1 and 2 to 5 and 6). We also observe a faster migrating band detected with the PARN antibody in the immunoblotting analyses. This band remained relatively unaffected upon overexpression of both miRNAs. Whether this represents a form of PARN that is differentially regulated by miRNAs remains an open question.

Furthermore, miR-29a-3p and miR-1207-5p were targeted with specific antisense locked nucleic acid (LNA) inhibitors in NCI-H520 cells for 24, 48, and 72 h. The subsequent qRT-PCR analysis demonstrates a significant up-regulation of PARN mRNA (Fig 4A). At the protein level, blocking of miR-29a-3p increased PARN levels (Fig 4B, compare lanes 1 and 2 to lanes 3 and 4, respectively), whereas miR-1207-5p impediment had minimal effect. These results show that miR-29a-3p and miR-1207-5p target PARN 3′UTR affecting PARN mRNA and protein levels. Collectively, the previous results reveal a dynamic relation between PARN and these miRNAs, miR-29a and miR-1207.

PARN precipitates with CPSF6

The previous results suggest that PARN is involved in the early steps of miR-29a maturation. To identify factors that associate with and could recruit PARN to polyadenylated pri-miR-29a transcripts, we performed immunoprecipitation experiments in extracts of NCI-H520 cells with PARN antibody, followed by mass spectrometry. Of the identified proteins, we focused on cleavage and

indicate the experimental time of treatments. White arrowheads and numbers in parentheses indicate time points of sampling after addition of ActD. **(B)** Levels of pri-miR-29a and miR-29a-3p upon inhibition of transcription. NCI-H520 cells were treansfected for PARN overexpression (left panel), PARN E30A (middle panel) and PARN silencing (right panel), then treated with ActD and the levels of pri-miR-29a and miR-29a-3p were measured by qRT-PCR at the indicated time points following treatment. Data points represent individual relative qRT-PCR measurements from at least two independent repetitions. **(C)** PARN precipitates with primary and mature forms of miR-29a. RNA immunoprecipitations with pre-immune and PARN polyclonal antisera were performed in NCI-H520 nuclear and cytoplasmic extracts and the associated RNA was subjected to qRT-PCR for pri-miR-29a (left panel) and miR-29a-3p (right panel). Pre, pre-immune antiserum; cyto, cytoplasmic fraction. **(D)** PARN affects the poly(A) status of pri-miR-29a. Design of the LM-PAT assay and relative hybridization positions of primers (upper panel). α and dT-12 anchor indicate position of primers (not in scale). LM-PAT assay (lower panel). NCI-H520 cell extracts 72 h-post transfection with empty vector (mock; lane 2) or PARN shRNA (lane 5) were analyzed. The arrowhead indicates the position of the minimal expected non-polyadenylated amplified product determined by the position of primer and the beginning of the poly(A) tail (~380 nt). Actin transcripts served as internal control (lanes 1, 4). M, molecular length markers (lane 3); sh PARN: 72 h-post PARN silencing.

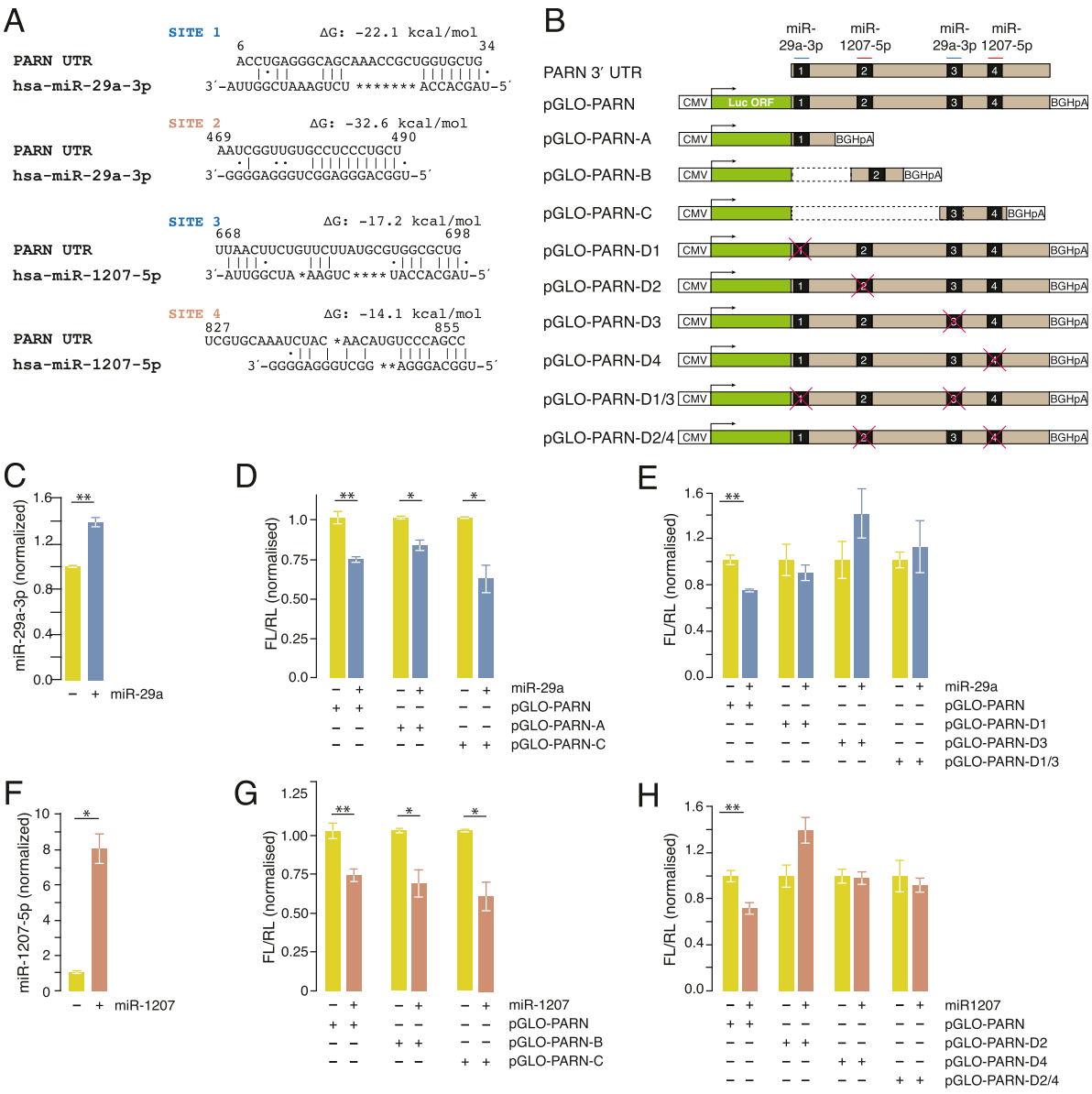

Figure 3. miR-29a-3p and miR-1207-5p target PARN 3′UTR and affect PARN mRNA levels.
(A) PARN 3′UTR, miRNA-29a-3p and miRNA-1207-5p target sites. **(B)** Luciferase reporter constructs used in the study. Numbered black boxes: predicted miRNAs hybridization to PARN 3′ UTR. Box numbers are the sites in Fig 4A. The miR-29a-3p and miR1207-5p sites are shown by a blue and a red line above the boxes, respectively. The PARN-UTR construct harbors the full 3′ UTR. Constructs harboring shorter 3′ UTRs (pGLO-PARN-D1–3) are shown; dotted boxes, deleted residues in the seed regions. pGLO-PARN-D1 to pGLO-PARN-D4, constructs with one miR-binding site mutation. pGLO-PARN-D1/3 and pGLO-PARN-D2/4, constructs with both miR-29a-3p or miR-1207-5p binding sites are mutated, respectively. **(C, D, E)** miR-29a-3p hybridizes to PARN 3′ UTR. **(C)** Overexpression of miR-29a-3p. HeLa cells were transfected with psiUx-miR-29a plasmid (blue column) and empty vector (yellow column). miR-29a-3p levels were measured 24-h post transfection. *P < 0.05; **P < 0.01. **(D)** Activity of Firefly Luciferase in HeLa cells cotransfected with the PARN-UTR reporters and miRNA overexpressing plasmids. Expression was measured 24-h posttransfection. *P < 0.05; **P < 0.01. Blue columns, transfections containing psiUx-miR-29a, for miR-29a-3p overexpression. **(E)** Activity of Firefly Luciferase in HeLa cells cotransfected with the indicated PARN-UTR reporters (wt and mutated forms) and miRNA overexpressing plasmids. *P < 0.05. **(F, G, H)** miR-1207-5p hybridizes to PARN 3′ UTR. **(F)** Overexpression of miR-1207-5p. HeLa cells were transfected with psiUx-miR-12075p plasmid (brown column) and empty vector (yellow column). miR-1207-5p levels were measured as in 3D. **(G)** Activity of Firefly Luciferase in HeLa cells cotransfected with PARN-UTR reporters and miRNA overexpressing plasmids. *P < 0.05, **P < 0.01. Pink columns indicate transfections containing plasmid psiUx-miR1207 to overexpress miR-1207-5p. **(H)** Activity of Firefly Luciferase in HeLa cells cotransfected with indicated PARN-UTR reporters (wt and deleted forms) and miRNA overexpressing plasmids. *P < 0.05. For each construct, the value of the transfection containing the empty plasmid was set to 1 (yellow columns). Values, normalized for expression of Renilla Luciferase are means ± SEM (n = 3). Luciferase expression was measured 24 h posttransfection.

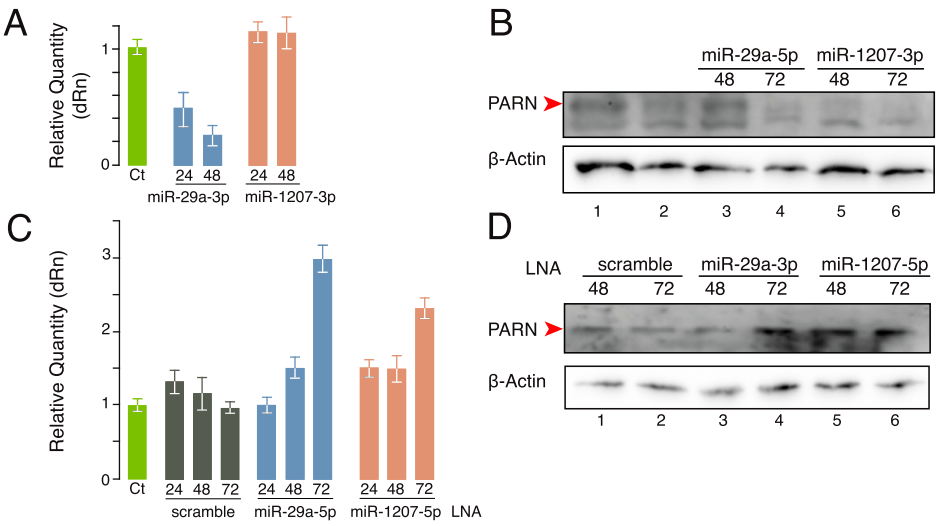

Figure 4. miR-29a and miR-1207 affect both PARN mRNA and protein levels.
(A, B) miR-29a-3p and miR-1207-5p overexpression down-regulate PARN mRNA and PARN protein. **(A)** qRT-PCR Relative Quantitive Chart representing PARN mRNA levels upon miR-29a-3p (blue columns) or miR-1207-5p (pink columns) overexpression. **(C)** Green bar indicates PARN mRNA levels from WT (not transfected) cells used for normalization. Numbers below the columns (24, 48) indicate hours post transfection. **(B)** Western blot showing PARN protein levels upon miR-29a-3p and miR-1207-5p overexpression 48 and 72 h post transfection. Extracts from WT (lane 1) and empty-vectortransfected H520 cells (lane 2) served as controls. β-actin was used as a loading reference. **(C, D)** miR-29a-3p and miR-1207-5p inhibition up-regulates PARN. **(C)** PARN mRNA levels in the presence of miR-29a-3p or miR-1207-5p LNAs in NCI-H520 cells. Cells were transfected with LNA against miR-29a-3p (blue columns) or LNA against miR-1207-5p (pink bars) and PARN mRNA levels were measured with qRT-PCR. A scramble LNA was used as a negative control (gray bars). **(C)** Green bar indicates PARN mRNA levels from WT (not transfected) cells used for normalization. Numbers below the columns indicate hours post transfection. **(D)** Levels of PARN protein upon transfection with LNAs against miR-29a-3p or miR-1207-5p. Numbers (48 and 72) above the lanes indicate hours post transfection. The type of LNAs is indicated above numbers: scramble, lanes 1 and 2; miR-29a-3p, lanes 3 and 4; miR-1207-5p, lanes 5 and 6. The red arrowhead indicates the position of 74-kD PARN (B, D).

polyadenylation specificity factor 6 (CPSF6) (Fig S3), the 68 kD larger component of the mammalian cleavage factor I (CFI_m), which is essential for the early steps of mRNA 3′ end processing and the selection of multiple poly(A) sites (Ruegsegger et al, 1996; Gruber et al, 2012).

To validate the interaction between PARN and CPSF6, we performed immunoprecipitation assays in NCI-H520 cell extracts treated with RNase A before washing to reduce potential RNA-mediated interactions. CPSF6 was recovered when PARN was immunoprecipitated, and vice versa, CPSF6 immunoprecipitation resulted in the detection of PARN (Fig 5A, lanes 1, 2 and 5, 6, respectively). Under these conditions PARN and CPSF6 co-precipitate, highlighting that their association is protein-mediated. Furthermore, experimentation will be necessary to define the interaction between PARN and CPSF6.

CPSF6 modulates primary miR-29a and miR-1207, and mature miR-29a-3p and miR-1207-5p levels

To acquire additional information on the impact of CPSF6 on pri-miR-29a and miR-29a-3p levels, we silenced or overexpressed CPSF6 in NCI-H520 cells. Upon CPSF6 silencing, pri-miR-29a and miR-29a-3p levels increased by ~3.5-fold and ~3-fold above control levels, respectively (Fig 5B). A similar impact was observed on pri-miR-1207 and miR-1207-5p levels, but to a lesser extent (Fig 5C). On the other hand, up-regulation of CPSF6 decreased pri-miR-29a levels at ~50%, whereas, a six-fold increase of mature miR-29a-3p levels was observed (Fig 5D).

These results show that CPSF6 regulates the expression levels of the selected transcripts and together with the immunoprecipitation data, suggest that CPSF6 and PARN may act in concert to mediate early maturation steps of pri-miR-29a and pri-miR-1207. Moreover, the PARN—CPSF6 interaction together with the observations that PARN precipitates with miR-29a-3p and affects its stability and its polyadenylation status suggest that the enzyme mediates an early step in the biogenesis pathway possibly before the microprocessor processing.

PARN, miR-29a-3p, and miR-1207-5p affect wound healing

Our results suggest the existence of a dynamic relation between PARN and miR-29a-3p that maintain their cellular levels. To investigate the biological significance of this relation, we investigated previous roles of PARN on cell motility in mouse myoblasts (Lee et al, 2012). We examined the impact of the migrating ability of NCI-H520 cells upon PARN silencing, overexpression, or expression of PARN E30A, as well as miR-29a-3p and miR-1207-5p overexpression or inhibition (Fig 6). Transfection with scramble shRNA (shscr) had minor effect on the migration of the cells when compared with untransfected cells (Fig 6A and C, compare wt with shscr columns), whereas transfection with empty pcDNA4 vector increased the migration index to ~25% (Fig 6C, compare wt and pcDNA4 columns). Upon PARN silencing the migration rate increased ~2-fold compared with the control (shscr; Fig 6A and C; compare silencing/shPARN and shscr). Overexpression of PARN or PARN E30A revealed healing rates of ~40% when compared with scramble shRNA (Fig 6A and C; compare overexpression/PARN and PARN E30A to shscr), or similar rates when compared with cells transfected with empty vector (pcDNA4; empty plasmid control) (Fig 6A and C; compare overexpression/PARN and PARN E30A to pcDNA4). Regarding the effect of the selected miRNAs on cell motility, miR-29a-3p or miR-1207-5p overexpression efficiently accelerated closure compared with control at ~3.5-fold (Fig 6B and D; compare miR-29a-3p and miR-1207-5p to psiUx). Treatment of the cells with specific LNAs for miR-29-3p or miR-1207a-5p resulted in ~30% and 50%, increase, respectively (Fig 6B and D; compare LNA miR-29-3p and LNA miR-1207a-5p to scrambled LNA; LNAscr).

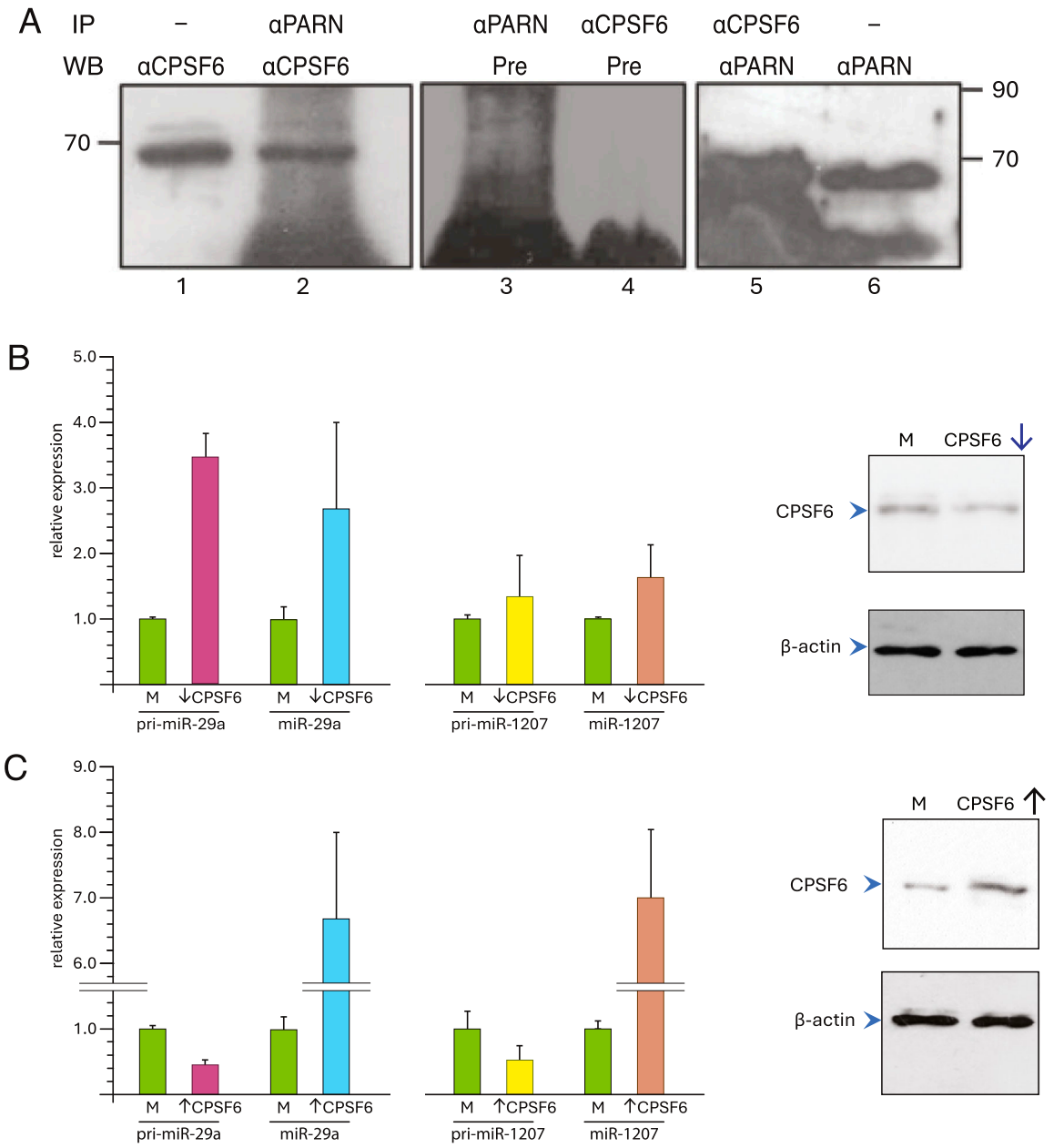

Figure 5. CPSF6 associates with PARN and affects the levels of miR-29a-3p and miR-1207-5p.
(A) Immunoprecipitation of NCI-H520 extracts with CPSF6 and PARN polyclonal antibodies and preimmune sera. Upon IP, the samples were subjected to RNase A treatment and analyzed by Western blot (WB) probed with PARN and CPSF6 antibodies, respectively, as indicated above the lanes. As an additional control both IP samples were probed with pre-immune-PARN 74 kD serum. αPARN, polyclonal PARN antibody; αCPSF6, polyclonal CPSF6 antibody; Pre, preimmune-PARN 74 kD serum. **(B, C)** Levels of pri-miR-29a and pri-miR-1207, mature miR-29a-3p and miR-1207-5p upon silencing (B) and overexpression (C) of CPSF6. The efficiency of silencing and up-regulation of CPSF6 was detected with CPSF6 antibody, shown on the right panel of B and C, respectively. Actin served as control and detected with actin antibody. Upward (↑) and downward (↓) arrows denote silencing and up-regulation of CPSF6, respectively. Mean values ± SD, n = 3. The arrowheads indicate the position of CPSF6 and β-actin.

Treatment of the cells with LNAscr delayed healing to rates comparable to the ones observed with empty vector (Fig 6B and D; compare LNAscr and psiUx). The previous results show that the highest migration rates were observed when PARN was silenced and miR-29a-3p was overexpressed. Regarding miR-1207-5p, overexpression resulted into a twofold acceleration of healing (Fig 6B and D, compare over miR-1207-5p to LNAscr). Blocking of miR-1207-5p resulted in comparable rates to its overexpression (Fig 6D, compare over- to LNA miR-1207-5p bars), possibly suggesting a different involvement in cell migration.

These results highlight the significance of miR-29a and the regulatory role of PARN in cell motility. When the levels of PARN are

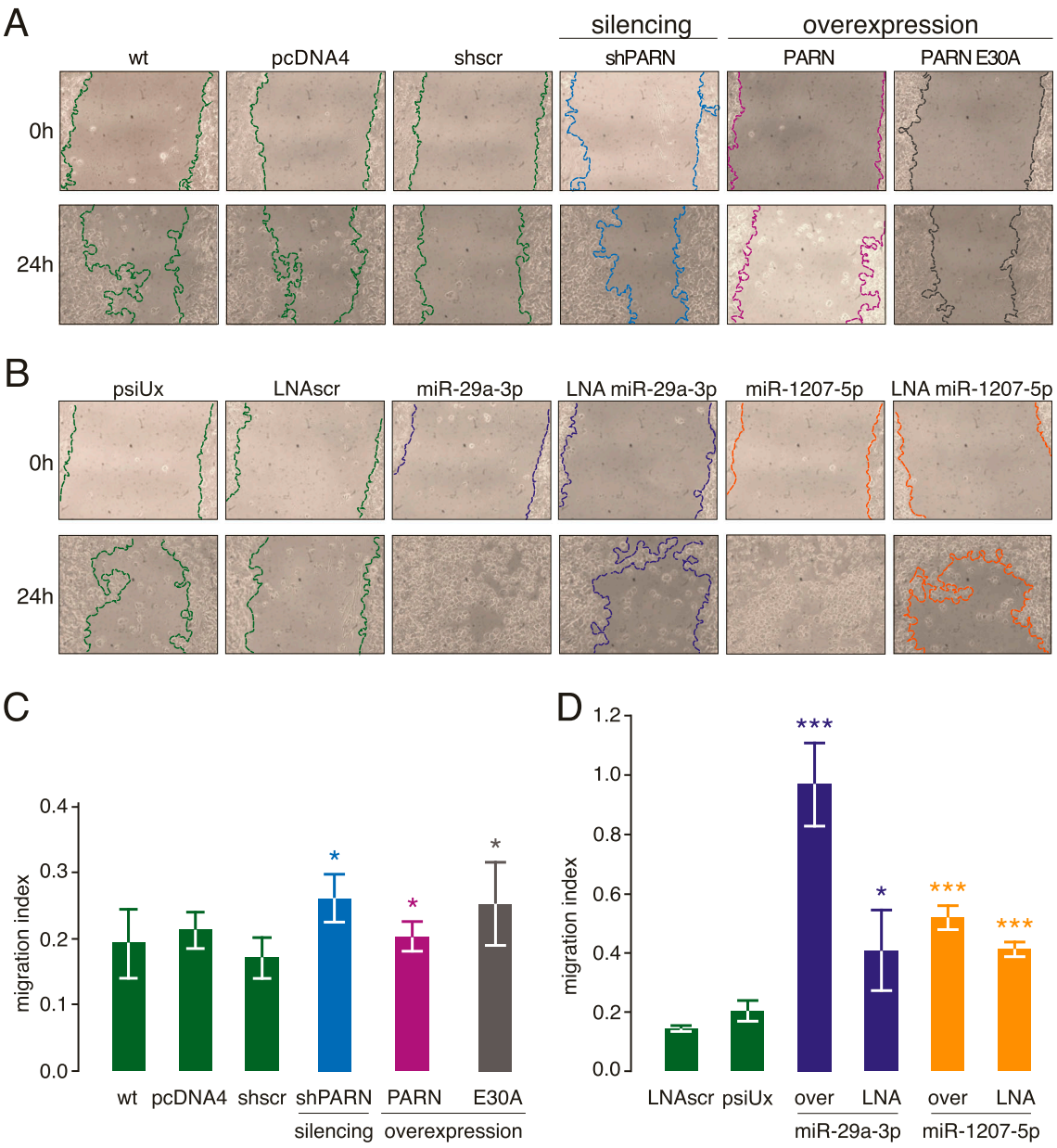

Figure 6. PARN, miR-29a-3p, and miR-1207-5p affect cell motility.
WT and transfected NCI-H520 cells were grown and a wound was made the healing was monitored over a period of 24 h. Brightfield images of the wounds (0 h) and healing process (24 h) are shown (n = 3). **(A)** Effect of PARN on NCI-H520 cell motility. PARN expression was silenced with shRNAs (silencing/shPARN). PARN or a catalytically inactive PARN (PARN E30A) were overexpressed. As controls, the following conditions were used: WT NCI-H520 cells (wt), cells transfected with empty vector (pcDNA4) and cells transfected with a scramble shRNA (shscr). **(B)** Effect of miR-29a-3p and miR-1207-5p on NCI-H520 cell motility. miR-29a-3p and miR-1207-5p were overexpressed (over) or blocked with LNAs (LNA miR-29a-3p and LNA miR-1207-5p, respectively). As controls, the following conditions were used: cells transfected with either empty plasmid (psiUx) or a scrambled LNA (LNAscr). **(C, D)** Migration indices of wound healing of the conditions studied in (A, B) are represented in (C, D), respectively. The migration index denotes the measured gap area. A migration index of 1 indicates full closure of the wound gap. Error bars represent the SD of triplicate wound healing assays.

low (upon silencing) the levels of miR-29a remain high (Figs 1B and C and 2B) and this is reflected in increased migration, which is also the case when miR-29a-3p is overexpressed (Fig 6B and D). When the levels of miR-29a-3p are high (i.e., upon overexpression), the levels of PARN are low and the migration is accelerated (as observed for PARN silencing in Fig 6C). Overall, PARN in cell motility seems to be manifested through a concerted action with miR-29a. As for miR-1207, the impact on wound healing was evident albeit to a lesser extent compared with miR-29a, implying that is involved in migration mechanisms driven by other factors.

Discussion

In this work, we investigate the impact of PARN in microRNA stability. We find that a subset of microRNAs is affected by PARN, including miR-29a-3p and miR-1207-5p. PARN precipitates with both primary and mature miR-29a and determines their stability, whereas the enzyme affects the poly(A) tail length of pri-miR-29a. On the other hand, miR-29a-3p and miR-1207-5p are predicted to target PARN mRNA. We validate the hybridization of miR-29a-3p or miR-1207-5p to the 3′ UTR of PARN mRNA and we further show that both miRs affect PARN mRNA and protein levels. To investigate for factors that recruit PARN on the primary miR forms, we find that the enzyme precipitates with CPSF6. The latter also affects pri- and mature miR-29a and miR-1207 levels, suggesting that CPSF6 recruits PARN to mediate early steps of miR biogenesis. The previous reveal a dynamic relation of PARN with miR-29a and miR-1207 to modulate bidirectionally their levels, mediated by CPSF6. Finally, we examine the biological impact of this relation in cell mobility.

miR biogenesis

Previous works on miRNA biogenesis revealed PARN as a mediator in the late steps of the process and, together with PAPD5, it maintains steady-state levels of noncoding nuclear RNAs by limiting their degradation via the nuclear exosome (Shukla et al, 2016, 2019; Lee et al, 2019). PARN mediates the biogenesis of most canonical miRNAs, whose maturation depends on DROSHA and DICER (Lee et al, 2019). It trims pre-miR-451 and the 3′ uridine or adenosine extensions, as well as miR-362-5p, to define their final length, suggesting a conserved mechanism in vertebrate miRNAs (Yoda et al, 2013; Lee et al, 2019), and catalyzes the turnover of adenylated microRNAs in the cytoplasm, including miR-21 and miR-122 (Boele et al, 2014; Katoh et al, 2015). Thus, PARN has been proposed to function as both a "trimmer" of 3′ extensions and a "de-tailor" to determine the size of untemplated nucleotide additions (Lee et al, 2019).

Consistent with this expanded role, the results presented here indicate that PARN also participates in early events of miR-29a biogenesis, possibly before the involvement of the microprocessor, as evidenced by the accumulation of pri-miR-29a and modest decreases (~8–12%) in mature miR-29a upon PARN silencing (Fig 2). These modest changes are consistent with the established role of miRNAs as fine-tuners of gene expression. Differences in the magnitude of fold-changes between the microarray and qRT-PCR measurements of miRNAs are well documented, including comparative work (Del Vescovo et al, 2013) and systematic analyses (Rachinger et al, 2021). These discrepancies arise from inherent methodological distinctions between the platforms: (i) microarrays rely on hybridization-based probe behavior, which can be influenced by variable affinity and cross-hybridization, whereas qRT-PCR uses specific primers; (ii) the two methods used different normalization strategies (global array normalization vs. reference gene normalization); and (iii) microarray probes may detect multiple isoforms or precursor species, whereas qRT-PCR typically amplifies a single mature miRNA. Together, these factors readily explain the larger dynamic range observed in array data and indicate that the differences we report reflect described platform-specific characteristics rather than experimental error. Importantly, the regulation is consistent in both methods, supporting the biological validity of our findings.

miRNAs typically modulate large sets of targets with small effects at each site, generating coordinated changes across regulatory networks that influence cellular phenotypes (Jonas & Izaurralde, 2015; Bartel, 2018). Single-cell and modeling studies indicate that miRNAs can establish threshold and nonlinear responses at individual targets, such that even modest average shifts in abundance can result in meaningful effects on target expression and downstream processes (Mukherji et al, 2011; Schmiedel et al, 2015). Moreover, miRNAs contribute to the stabilization of target transcripts and the reduction of expression noise, reinforcing their capacity to control gene expression precisely. In this context, the modest PARN-dependent modulation of miR-29a observed here is expected to have measurable regulatory consequences within cellular networks, supporting a model in which PARN primarily affects miRNA processing kinetics and efficiency rather than inducing large shifts in steady-state miRNA levels.

These data highlight a role for PARN in shaping the poly(A) status of pri-miR-29a, providing new insight into its early function in miRNA biogenesis and the basis for future studies on tail length regulation and enzymatic mechanism. Taken together, these observations broaden the roles of PARN as a guardian of miRNA biogenesis, acting from early processing steps described here through previously reported late maturation and turnover stages (Yoda et al, 2013; Boele et al, 2014; Katoh et al, 2015; Lee et al, 2019).

miR-29a and miR-1207 modulate PARN levels

The experimental results of luciferase showed that both miRs can bind the 3′UTR of PARN mRNA. Overexpression of miR-29-5p decreased both mRNA and protein levels (Fig 4). Overexpression of miR-1207 and subsequent Western blot analysis reflects on reduced protein levels of the enzyme, yet it has limited impact on mRNA levels. Although miRNAs are often considered post-transcriptional regulators that reduce target mRNA abundance, mechanistic studies show that unchanged mRNA levels do not preclude effective miRNA-mediated silencing; translational repression can precede or occur independently of mRNA decay. For instance, it has been demonstrated that miRNA-mediated inhibition of protein synthesis occurs before deadenylation and decay in *Drosophila* S2 cells (Djuranovic et al, 2012). Furthermore, miR-430 reduces ribosome occupancy on target mRNAs before significant transcript degradation, highlighting translational repression as an early regulatory step in zebrafish embryos (Bazzini et al, 2012). In vitro studies indicate that miRNAs can block translation during 43S ribosomal scanning without affecting mRNA stability (Ricci et al, 2013). Moreover, miRNAs can induce rapid deadenylation that does not immediately reduce mRNA levels, underscoring the temporal separation between translational repression and mRNA decay (Wu et al, 2006). Consistent with these mechanisms, our results show that miR-1207 primarily represses translation rather than promoting transcript degradation.

CPSF6 interaction

A plethora of factors and multisubunit complexes mediate the early steps of mRNA maturation, known as 3′ end processing. Among them, Cleavage stimulation Factor (CstF) together with Cleavage Factor Im (CFIm) and CPSF bind synergistically to pre-mature mRNA to assemble the core 3′ processing complex machinery of RNA polymerase II transcripts (Shi & Manley, 2015; Boreikaite & Passmore, 2023). Previous work has shown that PARN is present in the early steps of mRNA processing; it interacts with CstF50 to modulate mRNA 3′ cleavage and activation of deadenylation upon UV-induced DNA damage suggesting a mechanism to prevent the expression of prematurely terminated transcripts, thus contributing to the control of gene expression under different cellular conditions (Cevher et al, 2010).

The impact of PARN on pri-miR poly(A) tail (Fig 2), the accumulation of primary miRNA transcripts upon silencing (Fig 2) and the interaction with CPSF6, a factor involved in the very early steps of mRNA processing, suggest a prerequisite deadenylation step of the primary transcripts, short after cleavage and polyadenylation of the transcript. This could be attributed to the destabilization of the essential CPSF/RNA complex and/or any other inhibitory interaction into the complex 3′ end processing machinery, as has been previously proposed for the PARN—CstF50 interaction and subsequent impact (Cevher et al, 2010). Furthermore, research is necessary to uncover the full mechanism of this interaction.

The interaction of PARN with CPSF6 described in this work expands the repertoire of PARN partners and provides the basis to reveal its role in the early steps of primary miRNA processing. Although CPSF6 and PARN co-immunoprecipitate, the current data suggest that they are part of the same processing complex, yet further studies are needed to confirm a direct physical interaction between the proteins. Moreover, in light of independent reports on miRNA association with PARN and CPSF6, it may reveal important interlocking regulatory pathways. For instance, miR125b targets p53 mRNA and recruits PARN on it triggering destabilization of the transcripts and subsequent decrease in TP53 protein levels (Zhang et al, 2015). Moreover, miR125b physically interacts with CPSF6 mRNA modulating CPSF6 levels (Chaudhuri et al, 2020). Interestingly, TP53 regulates positively the PVT1 long noncoding RNA cluster coding for six annotated miRs including miR-1207 (Huppi et al, 2008; Barsotti et al, 2012; Colombo et al, 2015). Future work will elucidate whether PARN destabilizes CPSF6 mRNA through miR125b and reveal the exact regulatory interplay that modulate the levels of PARN, CPSF6, TP53, and miR-clusters as *PVT1*.

Cell migration

We observe that PARN and miR-29a-3p inversely modulate cell migration (Fig 5). As mentioned, PARN regulates cell motility in mouse myoblasts and negatively regulates cell migration (Lee et al, 2012). In a genome-wide analysis and gene ontology (GO) enrichment upon silencing of PARN in NCI-H520 cells up-regulated factors involved in cell migration as MALAT1, which in turn is dysregulated in many cancers, including non-small cell lung cancer (Lin et al, 2007a; Li et al, 2018; Kyritsis et al, 2022), as well as of GOs associated to cell junction adhesion that has been involved in epithelial-mesenchymal transition (EMT) and metastasis (Talbot et al, 2012; Kyritsis et al, 2022). Furthermore, wound healing assays in MDA-MB-231 cells of breast cancer origin showed that the silencing of the CFI_m25 subunit of CFI_m, promotes cell migration (Tamaddon et al, 2020), similar to our observation upon PARN silencing in NCI-H520 cells, whereas we also show that PARN interacts with the CPSF6 (CFI_m68) subunit of CFI_m. On the other hand, the miR-29 family has established roles in tumorigenesis and cancer progression (Mazzoccoli et al, 2018); miR-29a-3p has been reported to inhibit cell migration in a cell line of colorectal cancer origin (He et al, 2017) and hepatocellular carcinoma cells (Xiao et al, 2019). Yet, it is reported to enhance cell migration in nasopharyngeal carcinoma (Qiu et al, 2015), possibly through different regulatory mechanisms.

Taken together the results presented in this work with previous reports highlight a dynamic relation between PARN and miR-29a that reflects on cell migration; increased cell migration is observed when PARN levels are low and miR-29a-3p are high, whereas silencing of PARN and CPSF6 both increase pri-miR-29a and miR-29a-3p levels (Figs 2B and 3B and C). When cells are to move, high miR-29a-3p levels (as observed in Fig 5) maintain low levels of PARN and thus favor factors as MALAT1 to drive cell migration. Moreover, PARN, which interacts with CPSF6 (CFI_m68), and CFI_m25 negatively affect cell migration; it could be hypothesized that CPSF6 (or CFI_m) is a key factor that regulates the recruitment of PARN on targets as pri-miR-29, triggering downstream effect that lead to the modulation of the migratory process. Overall, our results of the wound healing experiments in NCI-H520 cells of lung cancer origin suggest that PARN and miR-29a may act in concert to modulate cell migration. Whether miR-29a targets mRNAs of factors associated with motility that are further destabilized by PARN or whether PARN acts in concert with CPSF6 or other components of the CFIm complex in cancer remain open questions. Clearly, further experimental work will elucidate the role of these factors in the mechanisms that drive cell migration and metastasis.

A dynamic relation between PARN and miR-29 that regulates their expression

In this work, we show that upon transcription of miR-29a gene, the primary transcripts associate with PARN (Fig 2B and C), which modulates their poly(A) status (Fig 2D). This step is important for further maturation of pri-miR-29a; silencing of PARN results in accumulation of unprocessed pri-miR-29a transcripts and reduced levels of miR-29a as they are not replaced by newly matured transcripts, whereas the opposite observations resulted when the levels of the enzyme increase (Fig 2B).

CPSF6 mediates the recruitment of PARN on pri-miR-29a (Fig 3). In the absence of CPSF6, pri-miR-29a accumulates, whereas overexpression of the factor reduces the levels of primary transcripts and markedly increased the levels of mature miR-29a (Fig 3C and D). On the other hand, miR-29a targets PARN mRNA, reducing its protein levels (Fig 4) and interacts with PARN protein in the cytoplasm (Fig 2C). PARN also binds its own mRNA (Fig S2), suggesting an autoregulatory feedback layer.

Together, these results support a model for a dynamic relationship between PARN and miR-29a (outlined in the Graphical

Abstract, where the phases of the relationship are indicated by numbers). As transcription of miR-29a gene proceeds, PARN is recruited by CPSF6 onto pri-miR-29a transcripts in the nucleus, which is further matured to miR-29a (phases 1, 2). miR-29a-3p, in turn, triggers down-regulation of PARN mRNA in the cytoplasm, which is reflected in reduced PARN protein levels, possibly involving autoregulation by binding to its own mRNA (phase 3). As a result of low PARN levels, pri-miR-29a accumulates and maturation to miR-29a is hampered (phase 4), resulting in low levels of miR-29a (phase 5). This, in turn, rescues newly transcribed PARN mRNA allowing for synthesis and accumulation of PARN protein (phase 6) thereby initiating the maturation of primary miR-29a transcripts (phase 1).

Materials and Methods

Cell culture

NCI-H520 cells of non-small-cell lung cancer (NSCLC) origin were reconstituted and cultured in RPMI medium (Biosera). All cell lines were supplemented with 10% FBS (Biosera) and 1% antibiotic/antimycotic (XC-A4110). All cell culture reagents were purchased from Biosera (France). The cells were cultured at 37°C, in 5% CO_2 environment and were checked frequently for mycoplasma infection by PCR.

miRNA microarray analysis

Cells were collected and lysed. Total RNA isolation was performed using TRIzol Reagent (Sigma-Aldrich). 100 ng of total RNA samples was processed and hybridized to Human miRNA V2 Microarray 8x15K (G4470B; Agilent Technologies) using the miRNA Microarray System labeling kit V2 (Agilent 5190-0456), according to the manufacturer's instructions. Hybridized microarray slides were scanned with an Agilent DNA Microarray Scanner G2505C, and data were analyzed with the Agilent ScanControl version 8.1.3 software. The scanned TIFF images were background corrected using the Agilent Feature Extraction Software version 10.7.7.1. The raw data were normalized to the 75th percentile signal intensity as recommended by the vendor. After normalization all negative signal values were replaced by 0.01 and the values from multiple replicate spots for each miRNA were summarized as median signals which were used subsequently for statistical analyses. The pairwise Welch's *t* test was used to identify significantly deregulated miRNAs.

The raw data were normalized by quantile normalization method. Among 1,369 detectable spots 193 miRNAs were detected at least in one condition; 96 miRNAs in all conditions; 113 in all scramble shRNA replicates; 109 in all PARN silenced replicates. 43 miRNAs were deregulated (−0.5 > log [PARN/MSH] > 0.5) after PARN silencing: 12 down-regulated and 23 up-regulated.

In silico miR target prediction

To predict putative miRNAs' targets, we used TargetScan (http://www.targetscan.org) (Agarwal et al, 2015), miRDB (http://www.mirdb.org) (Chen & Wang, 2020), PITA (https://genie.weizmann.ac.il/pubs/mir07/mir07_prediction.html) (Kertesz et al, 2007), and TargetProfiler (https://mirna.imbb.forth.gr/Targetprofiler.html) (Oulas et al, 2012).

The hybridization minimum free energy (DeltaG) for miRNAs' binding was calculated with RNAhybrid (https://bibiserv.cebitec.uni-bielefeld.de/rnahybrid/) (Rehmsmeier et al, 2004).

Plasmid construction and cloning

For the overexpression experiments, the cDNA of human CPSF6 and PARN were cloned into the tetracycline-inducible pcDNA4/TO plasmid vector (T-Rex System; Invitrogen) using the HD In-Fusion Cloning kit (Takara Bio) according to the manufacturer's instructions. pcDNA4/TO-PARN E30A was generated by introducing a mutation of glutamate to alanine with specific mutagenic primers, as has been described previously (Beta et al, 2020). For the overexpression of miRNAs, the precursor regions of miR-1207 and miR-29a were PCR-amplified, using human genomic DNA as a template (Promega) and the forward and reverse primers reported, and ligated in the psiUx vector (Denti et al, 2004; Mancini et al, 2021) under the control of the U1 promoter. All plasmids were checked through restriction mapping and DNA sequencing.

PARN silencing and overexpression

The following short hairpin DNA plasmids were used to silence PARN: PARN (NM_002582) in NCIH520 cells and non-targeting control (SHC016), and the transfection was performed as described previously (Maragozidis et al, 2015) and according to the manufacturer (MISSION shRNA; Sigma-Aldrich). Silencing efficiency was determined by comparing PARN mRNA levels in cells transfected with the appropriate shRNAs against those that were transfected with nontarget shRNA. Expression levels were normalized to β-actin.

For PARN overexpression, the following constructs were used to transfect NCI-H520 cells: pcDNA4/TO-PARN and pcDNA4/TO-PARN E30A (T-Rex System; Invitrogen). PARN and PARN E30A overexpression efficiency was determined by comparing PARN levels in cells transfected with pcDNA4/TO-PARN and pcDNA4/TO-PARN E30A constructs, respectively, against those that were transfected with pcDNA4/TO empty vector after expression levels had been normalized to β-actin.

CPSF6 silencing and overexpression

CPSF6 was silenced in NCI-H520 cells with specific shRNAs (NM_007007; Sigma-Aldrich) using cationic liposomes (X-fect; Clontech). NCI-H520 cells were cultured in 12-well plates up to a confluency of 90–95% and were subsequently transfected with 2 μg plasmid per well. Puromycin selection (6 μg/ml) and harvesting were performed 12 and 72 h after transfection, according to the manufacturer. Cells transfected with scrambled shRNA (NM_001025356; Sigma-Aldrich) served as control. The efficiency of silencing was evaluated by qRT-PCR and Western blot analyses. pcDNA4-CPSF construct and pcDNA6/TR regulatory vector were

cotransfected at a ratio of 1:6 (wt:wt) in NCI-H520 cells, using cationic liposomes (X-fect; Takara Bio). The cells were harvested 24 h after tetracycline induction (200 ng/ml).

miRNA inhibition

For miRNA-29a-3p and miR-1207-5p inhibition, specific antisense oligonucleotides (based on Locked Nucleic Acid technology, LNA, Exiqon) were transfected in NCI-H520 cells, using cationic liposomes (siRNA X-fect; Clontech) for 72 h. A scramble LNA served as control.

RNA isolation, reverse transcription, and qRT-PCR

For qRT-PCR analysis of mature miRNAs and mRNAs, total RNA was extracted from NCI-H520 using the miNucleoSpin miRNA kit (Macherey-Nagel). For the detection of specific miRNAs and mRNAs, 1 μg of total RNA was used for cDNA synthesis with Mir-X miRNA First Strand Synthesis Kit (TaKaRa Bio) and PrimeScript first strand cDNA synthesis kit (TaKaRa Bio), respectively. The qRT-PCR was performed in the Mx3005P Real-Time PCR System (Stratagene) using KAPA SYBR Fast Universal qPCR kit (KAPA Biosystems). miRNA and mRNA expression levels were normalized to U6 snRNA and β-actin, respectively (Maragozidis et al, 2012, 2015).

For the miRNA transfected HeLa cells, total RNA was extracted using TRIzol reagent (Invitrogen) and reverse-transcribed using miRCURY LNATM Universal cDNA Synthesis kit II (Exiqon) according to the manufacturer's protocol. For qRT-PCR analysis of overexpressed miRNAs, total RNA was extracted from transfected HeLa cells line using TRIzol (Invitrogen), according to the manufacturer's instructions. Total RNA was then reverse-transcribed using miRCURY LNA Universal cDNA Synthesis kit II (Exiqon), miRCURY LNA PCR primers set for U6 snRNA (Assay ID: 203907), hsa-miR-1207-5p (Assay ID: 204693) and hsa-miR-29a-3p (Assay ID: 202118) were purchased from Exiqon. qRT-PCR reactions were performed using ExiLENT SYBR Green master mix (Exiqon) in a CFX384 qRT-PCR Detection System (Bio-Rad Laboratories). Samples were amplified in triplicate and quantification of relative expression was performed using the $\Delta\Delta C_T$ method. The amplified miRNA and mRNA products were separated in 4% and 1.5% agarose gel, respectively.

RNA immunoprecipitation

NCI-H520 cells were grown in T75-flasks and harvested at ~90% confluency. Cytoplasmic and nuclear fractions were treated with formaldehyde to stabilize protein–RNA interactions. Immunoprecipitations with pre-immune and PARN polyclonal antisera were performed according to standard procedures (Hendrickson et al, 2008, 2009). Finally, the associated RNA was extracted with TRI-Reagent (Sigma-Aldrich) and subjected to qRT-PCR with specific primers for miR-29a-3p and pri-miR-29a. The antibodies used in this work are listed in Table S1.

Immunoprecipitation

Immunoprecipitation assays were performed according to previously described protocols (McKendrick et al, 2001; Balatsos et al, 2006). Briefly, NCI-H520 cell extracts were subjected to immunoprecipitation using PARN and CPSF6 polyclonal antibodies as well as pre-immune serum as negative control. The extracts were precleared with 50 μl of protein A-Sepharose CL-4B beads (Acris Antibodies) at 4°C for 1 h with rotation followed by centrifugation at 10,000*g* in 4°C for 10 min. The cleared supernatant was diluted fivefold in IP150 buffer (20 mM Hepes, pH 7.9, 150 mM KCl, 0.05% Nonidet P-40, and 1% Triton X-100) and incubated with an appropriate volume of the antibody/pre-immune serum in 4°C for 1 h with rotation. Subsequently, the protein A-Sepharose beads were recovered by centrifugation and incubated at 4°C with 50 μg of RNase A/ml for 10 min. Finally, the beads were washed three times with 1 ml of ice-cold IP150 buffer, then eluted with SDS–PAGE sample buffer and the recovered proteins were resolved by SDS–PAGE.

Mass spectrometry analysis

NCI-H520 cell lysates were subjected to immunoprecipitation with PARN antiserum. The samples were resolved by SDS–PAGE electrophoresis and visualized with silver staining.

In-gel tryptic digestion of selected cut bands was performed according to standard procedures (Shevchenko et al, 1996). Briefly, the gel pieces were destained, dehydrated with acetonitrile and then rehydrated with 25 mM ammonium bicarbonate buffer. After repeating the dehydration with acetonitrile and rehydration with 25 mM ammonium bicarbonate buffer followed by dehydration with acetonitrile, the dried gel pieces were rehydrated with 12.5 ng/μl trypsin (Trypsingold; Promega) in 25 mM NH_4HCO_3 buffer and incubated over night at 37°C. Peptides were extracted from the gel with 100 μl extraction buffer 1:2 (vol/vol) 5% formic acid/acetonitrile for 30 min at 37°C, and the solution was transferred and dried in a vacuum centrifuge. Finally, the samples were reconstituted in 2% (vol/vol) acetonitrile/0.1% (vol/vol) formic acid and sonicated in a water bath for 5 min.

LC–MS/MS analysis

The purified peptides were analyzed by HPLC-tandem MS/MS using a C-18 column coupled to an LTQ Orbitrap XL Mass spectrometer (Thermo Fisher Scientific). 10 μl of peptides were pre-concentrated at a flow of 5 μl/min for 10 min using a C18 trap column (Acclaim PepMap RSLC; Thermo Fisher Scientific) and then loaded onto a 15 cm C18 column (75 μm ID, particle size 2 μm, 100 Å, Acclaim PepMap RSLC; Thermo Fisher Scientific). The binary pumps of the HPLC (RSLCnano; Thermo Fisher Scientific) contained solution A (2% [vol/vol] ACN in 0.1% [vol/vol] formic acid) and solution B (80% ACN in 0.1% formic acid). The peptides were separated using a linear gradient of 4–40% B in 55 min at a flow rate of 300 nl/min. The column was placed in an oven operating at 35°C. Full scan MS spectra were acquired in the orbitrap (m/z 300–1,600) in profile mode and data-dependent acquisition with the resolution set to 60,000 at m/z 400 and automatic gain control target at 10^6. The six most intense ions were sequentially isolated for collision-induced MS/MS fragmentation (normalized CID of 35%) and detection in the linear ion trap. Dynamic exclusion was set to 60 s. Ions with single charge states were excluded. Lockmass of m/z 445,120,025 was

used for internal calibration. The software Xcalibur (Thermo Fisher Scientific) was used to control the system and acquire the raw files.

Protein data analysis and database search

Peptides were identified using the Proteome Discoverer 1.4 software tools. The Orbitrap raw data (peak S/N threshold was set to 1.5) were searched using SEQUEST HT against the UniProt human FASTA database (70,173 entries, 10/2015) with strict trypsin specificity and with maximum two missed cleavages and variable modifications of methionine oxidation, deamidation of glutamine and asparagine residues and acetylation of the N-terminus. The peptides were filtered based on their Xcorr values versus peptide charge states (XCorr >1.9 for charge state +2 and XCorr >2.5 for charge state +3).

Actinomycin D treatment, and measurements of primary and mature miRNA levels

pri-miRNA-29a and miR-29a-3p decay rates were determined upon PARN silencing or overexpression using a qRT-PCR-based assay. NCI–H520 cells were grown to near confluency and deprived of serum for 24 h to be cell cycle synchronized before transfection (Cai et al, 2017). Actinomycin D, a general transcription inhibitor, was added to cells at a final concentration of 5–10 μg/ml 72 h post transfection. Total RNA was isolated from cells harvested at various time points (0, 1, 2, 4, 8, and 12 h) after actinomycin D addition using TRI Reagent following the instructions of the manufacturer (Sigma-Aldrich). RNA concentration was determined by spectrophotometry (NanoDrop 2000; Thermo Fisher Scientific). One microgram of total RNA was reverse-transcribed by Moloney murine leukemia virus (M-MuLV) reverse transcriptase (PrimeScript RT–PCR kit; Clontech) using $oligo_{12–18}$ as the reverse transcription primer. cDNA equivalent to 20 ng of total RNA was subjected to qRT-PCR using specific primers for miRNA-29a, pri-miRNA-29a. Data were normalized to values of empty vectors (pcDNA for PARN and PARN E30A overexpression and non-targeting control SHC016 for PARN silencing) at the indicated time points and represent measurements from at least two independent experiments.

Luciferase reporters

To generate the pGLO-PARN Dual-Luciferase miRNA reporter, the full-length 3′UTR of human PARN mRNA (positions 2067-3083, NM_002582.3) was generated by RT–PCR using HeLa cDNA as a template and the amplified fragment was cloned into SacI and XhoI sites present in pmirGLO plasmid (Promega). Similarly, shorter portions of the human PARN 3′UTR were generated by RT–PCR using HeLa cDNA as a template and cloned in pmirGLO SacI-XhoI sites. A deleted pGLO-PARN lacking eight bases of the miRNA seed region in each miRNA-binding site was created starting from pGLO-PARN and using a Quick-Change II XL Site-Directed Mutagenesis Kit (Stratagene), according to the manufacturer's protocol. pGLO-PARN-D1/D3 and pGLO-PARN-D2/D4, bearing two deletions, were created by further sitedirected mutagenesis of plasmids pGLO-PARN-D1 and pGLO-PARN-D2, respectively. All plasmids were checked through restriction mapping and DNA sequencing. All primer sequences are in Table S2.

Luciferase assay

HeLa cells per well were seeded in 24-well dishes and transfected at 80% confluence using TransITLT1 transfection reagent (MIRUS BIO) with 50 ng of the pGLO vector and 500 ng of miRNA overexpressing plasmids. The pGLO vector is designed to analyze miRNA activity by the insertion of miRNA target sites downstream of the firefly luciferase gene (luc2). miRNA-binding to the target sequence will produce a reduced firefly luciferase expression. Twenty-four hours after transfection cells were lysed with Luciferase Assay Reagent (Promega), and Renilla and Firefly luciferase activity were measured using Dual-Glo Luciferase Assay System (Promega) in the Infinite M200 (Tecan) plate reader.

Western blot

Cells were collected and protein isolation followed by using the TRIzol Reagent kit (Sigma-Aldrich). Protein concentration was measured using the BCA method. A total of 20 μg of protein was loaded into 10% SDS–PAGE gel for analysis. The bound antibodies were detected with an ECL Plus Western blotting Detection system (Amersham), and the chemiluminescent signals were detected by high-performance chemiluminescence film (GE Healthcare). Protein bands were normalized using ImageJ (Rueden et al, 2017).

Ligation-mediated polyadenylation test (LM-PAT)

LM-PAT was performed for the determination of the poly(A) tail length of pri-miRNA-29a, as described previously (Salles et al, 1999; Beilharz & Preiss, 2007) with some modifications. The isolation of RNA from NCI-H520 cells was performed using TRI-Reagent (Sigma-Aldrich), followed by DNase treatment to remove any contaminating DNA and purification with 5 M ammonium acetate and phenol/chloroform/isoamyl alcohol. For the LM-PAT cDNA synthesis, 250 ng of total RNA diluted in 5 μl of DEPC-treated water was mixed with 2 μl of phosphorylated $oligo_{18}$ (10 ng/μl) and incubated at 65°C for 10 min. The reaction was transferred immediately to 42°C in a mixture of RNase inhibitor (40 U/μl), 0.1 M DTT, 10 mM dNTP mixture, 5′ PrimeScript RT buffer (Takara), 10 Mm ATP, T4 DNA ligase (6–40 U) followed by 30 min incubation. Then, the $oligo_{18}$ anchor (200 ng/μl) was added in the reaction at 42°C, and samples were transferred to 12°C for 2 h. The mixture was then transferred to 42°C and was further incubated with PrimeScript Reverse Transcriptase (10 U/μl, Takara) (preheated at 42°C) for 1 h. Reverse transcriptase and T4 ligase were inactivated at 65°C for 20 min. LM-PAT cDNA was used (1–3 μl) as template for amplification by PCR. The primers used were specific to pri-miR-29a (forward primer *a*, Figure LM-PAT) and the $oligo_{18}$ anchor primer (reverse). PCR cycling conditions were: 94°C for 2 min, 30 cycles at 94°C/1 min, 57°C/30 s and 72°C/2 min, followed by a final extension step at 72°C for 7 min. The PCR products were

analyzed by electrophoresis on a 2.5% high-resolution agarose-TBE gel stained with Midori Green Advance DNA stain (Nippon Genetics). For primer sequences, see Table S2.

Wound healing assay

NCI-H520 cells (1.5×10^5 cells) were seeded in 24-well plates. A reference line was drawn on the bottom of the 24-well plate through each well with a fine point permanent marker before plating cells. The cell cultures were serum-starved before transfection to achieve basic synchronization, and once cultures approached confluency, a scratch perpendicular to the reference line was introduced with a pipette tip to create cell-free stripes (wounds). Digital images were taken immediately after and 24 h post wounding (Leica Application Suite Version 3.4.0). Microscopy was performed with an inverted microscope. Cell migration index was introduced to measure the cells' ability to heal the wound and computed using the following formula: Migration Index = $(A_{0h} - A_{24h})/A_0$, where A denotes the gap area measured. A migration index of 1 indicates full closure of the wound gap.

Data Availability

Raw data have been deposited in NCBI's Gene Expression Omnibus (https://www.ncbi.nlm.nih.gov/geo) and are available under accession number GSE207372. The mass spectrometry analysis is deposited in ProteomeXchange via the PRIDE database (Project Accession: PXD064050).

Supplementary Information

Supplementary Information is available at https://doi.org/10.26508/lsa.202503341.

Acknowledgements

This work was partially supported by a grant of the Hellenic Thoracic Society (NAA Balatsos; Grant number 8000, University of Thessaly Research Committee) and the University of Thessaly Postgraduate Programs 3439 "Biotechnology - Quality Assessment in Nutrition and the Environment" and 3817 "Applications of Molecular Biology- Genetics - Diagnostic Biomarkers" of the Department of Biochemistry and Biotechnology (NAA Balatsos). This work is supported by the Ministry of Development and Investments Operational Programme: "Supporting researchers with Education and Lifelong Learning" in the context of the project: "Supporting researchers focusing on young researchers-103" (MIS 5048947) (NSRF 2014–2020). A Kyritsis is recipient of a State Scholarships Foundation (IKY) Fellowship of Excellence for Postgraduate Studies in Greece—Siemens Programme. We wish to acknowledge the Staff of the High-Throughput Facility of the Department CIBIO at the University of Trento for the microarray experiments. MA Denti acknowledges funding by the Department CIBIO, University of Trento, and by EU MSCA-RISE GA 690866. K Papikinos was recipient of an Erasmus Fellowship. MA Denti and NAA Balatsos acknowledge financial support by EU MSCA-RISE GA 101007934.

Author Contributions

A Kyritsis: supervision, methodology, and writing—review and editing.
RAA Beta: methodology and writing—review and editing.
D Scutelnic: methodology and writing—review and editing.
V Stravokefalou: methodology.
V Del Vescovo: supervision and methodology.
ZV Arsenopoulou: methodology.
K Papikinos: methodology.
M Grasso: supervision and methodology.
F Fontana: methodology.
P Moutopoulou: methodology.
A Tsiporis: methodology.
M Samiotaki: data curation, methodology, and writing—review and editing.
G Panayotou: methodology and writing—review and editing.
MA Denti: resources, supervision, funding acquisition, methodology, and writing—review and editing.
NAA Balatsos: conceptualization, resources, supervision, funding acquisition, methodology, and writing—original draft, review, and editing.

Conflict of Interest Statement

The authors declare that they have no conflict of interest.

References

Agarwal V, Bell GW, Nam JW, Bartel DP (2015) Predicting effective microRNA target sites in mammalian mRNAs. *Elife* 4: e05005. doi:10.7554/eLife.05005

Babiarz JE, Ruby JG, Wang Y, Bartel DP, Blelloch R (2008) Mouse ES cells express endogenous shRNAs, siRNAs, and other microprocessor-independent, dicer-dependent small RNAs. *Genes Dev* 22: 2773–2785. doi:10.1101/gad.1705308

Bail S, Swerdel M, Liu H, Jiao X, Goff LA, Hart RP, Kiledjian M (2010) Differential regulation of microRNA stability. *RNA* 16: 1032–1039. doi:10.1261/rna.1851510

Balatsos NA, Nilsson P, Mazza C, Cusack S, Virtanen A (2006) Inhibition of mRNA deadenylation by the nuclear cap binding complex (CBC). *J Biol Chem* 281: 4517–4522. doi:10.1074/jbc.M508590200

Barsotti AM, Beckerman R, Laptenko O, Huppi K, Caplen NJ, Prives C (2012) p53-dependent induction of PVT1 and miR-1204. *J Biol Chem* 287: 2509–2519. doi:10.1074/jbc.M111.322875

Bartel DP (2018) Metazoan MicroRNAs. *Cell* 173: 20–51. doi:10.1016/j.cell.2018.03.006

Bazzini AA, Lee MT, Giraldez AJ (2012) Ribosome profiling shows that miR-430 reduces translation before causing mRNA decay in zebrafish. *Science* 336: 233–237. doi:10.1126/science.1215704

Beilharz TH, Preiss T (2007) Widespread use of poly(A) tail length control to accentuate expression of the yeast transcriptome. *RNA* 13: 982–997. doi:10.1261/rna.569407

Berndt H, Harnisch C, Rammelt C, Stohr N, Zirkel A, Dohm JC, Himmelbauer H, Tavanez JP, Huttelmaier S, Wahle E (2012) Maturation of mammalian H/ACA box snoRNAs: PAPD5-dependent adenylation and PARN-dependent trimming. *RNA* 18: 958–972. doi:10.1261/rna.032292.112

Beta RAA, Kyritsis A, Douka V, Papanastasi E, Rizouli M, Leonidas DD, Vlachakis D, Balatsos NAA (2020) Biochemical and in silico identification of the active site and the catalytic mechanism of the circadian deadenylase HESPERIN. *FEBS Open Bio* 12: 1036–1049. doi:10.1002/2211-5463.13011

Boele J, Persson H, Shin JW, Ishizu Y, Newie IS, Sokilde R, Hawkins SM, Coarfa C, Ikeda K, Takayama K, et al (2014) PAPD5-mediated 3′ adenylation and subsequent degradation of miR-21 is disrupted in proliferative disease. *Proc Natl Acad Sci U S A* 111: 11467–11472. doi:10.1073/pnas.1317751111

Boreikaite V, Passmore LA (2023) 3′-end processing of eukaryotic mRNA: Machinery, regulation, and impact on gene expression. *Annu Rev Biochem* 92: 199–225. doi:10.1146/annurev-biochem-052521-012445

Cai J, Fang L, Huang Y, Li R, Xu X, Hu Z, Zhang L, Yang Y, Zhu X, Zhang H, et al (2017) Simultaneous overactivation of Wnt/beta-catenin and TGFbeta signalling by miR-128-3p confers chemoresistance-associated metastasis in NSCLC. *Nat Commun* 8: 15870. doi:10.1038/ncomms15870

Cazalla D, Xie M, Steitz JA (2011) A primate herpesvirus uses the integrator complex to generate viral microRNAs. *Mol Cell* 43: 982–992. doi:10.1016/j.molcel.2011.07.025

Cevher MA, Zhang X, Fernandez S, Kim S, Baquero J, Nilsson P, Lee S, Virtanen A, Kleiman FE (2010) Nuclear deadenylation/polyadenylation factors regulate 3′ processing in response to DNA damage. *EMBO J* 29: 1674–1687. doi:10.1038/emboj.2010.59

Chaudhuri E, Dash S, Balasubramaniam M, Padron A, Holland J, Sowd GA, Villalta F, Engelman AN, Pandhare J, Dash C (2020) The HIV-1 capsid-binding host factor CPSF6 is post-transcriptionally regulated by the cellular microRNA miR-125b. *J Biol Chem* 295: 5081–5094. doi:10.1074/jbc.ra119.010534

Chen Y, Wang X (2020) miRDB: An online database for prediction of functional microRNA targets. *Nucleic Acids Res* 48: D127–D131. doi:10.1093/nar/gkz757

Chong MM, Zhang G, Cheloufi S, Neubert TA, Hannon GJ, Littman DR (2010) Canonical and alternate functions of the microRNA biogenesis machinery. *Genes Dev* 24: 1951–1960. doi:10.1101/gad.1953310

Chou CF, Mulky A, Maitra S, Lin WJ, Gherzi R, Kappes J, Chen CY (2006) Tethering KSRP, a decay-promoting AU-rich element-binding protein, to mRNAs elicits mRNA decay. *Mol Cell Biol* 26: 3695–3706. doi:10.1128/MCB.26.10.3695-3706.2006

Colombo T, Farina L, Macino G, Paci P (2015) PVT1: A rising star among oncogenic long noncoding RNAs. *Biomed Res Int* 2015: 304208. doi:10.1155/2015/304208

Dehlin E, Wormington M, Körner CG, Wahle E (2000) Cap-dependent deadenylation of mRNA. *EMBO J* 19: 1079–1086. doi:10.1093/emboj/19.5.1079

Del Vescovo V, Meier T, Inga A, Denti MA, Borlak J (2013) A cross-platform comparison of affymetrix and Agilent microarrays reveals discordant miRNA expression in lung tumors of c-Raf transgenic mice. *PLoS One* 8: e78870. doi:10.1371/journal.pone.0078870

Denti MA, Rosa A, Sthandier O, De Angelis FG, Bozzoni I (2004) A new vector, based on the PolII promoter of the U1 snRNA gene, for the expression of siRNAs in mammalian cells. *Mol Ther* 10: 191–199. doi:10.1016/j.ymthe.2004.04.008

Dhanraj S, Gunja SM, Deveau AP, Nissbeck M, Boonyawat B, Coombs AJ, Renieri A, Mucciolo M, Marozza A, Buoni S, et al (2015) Bone marrow failure and developmental delay caused by mutations in poly(A)-specific ribonuclease (PARN). *J Med Genet* 52: 738–748. doi:10.1136/jmedgenet-2015-103292

Djuranovic S, Nahvi A, Green R (2012) miRNA-mediated gene silencing by translational repression followed by mRNA deadenylation and decay. *Science* 336: 237–240. doi:10.1126/science.1215691

Ender C, Krek A, Friedlander MR, Beitzinger M, Weinmann L, Chen W, Pfeffer S, Rajewsky N, Meister G (2008) A human snoRNA with microRNA-like functions. *Mol Cell* 32: 519–528. doi:10.1016/j.molcel.2008.10.017

Gao M, Fritz DT, Ford LP, Wilusz J (2000) Interaction between a poly(A)-specific ribonuclease and the 5′ cap influences mRNA deadenylation rates in vitro. *Mol Cell* 5: 479–488. doi:10.1016/s1097-2765(00)80442-6

Gherzi R, Lee KY, Briata P, Wegmuller D, Moroni C, Karin M, Chen CY (2004) A KH domain RNA binding protein, KSRP, promotes ARE-directed mRNA turnover by recruiting the degradation machinery. *Mol Cell* 14: 571–583. doi:10.1016/j.molcel.2004.05.002

Gregory RI, Yan KP, Amuthan G, Chendrimada T, Doratotaj B, Cooch N, Shiekhattar R (2004) The microprocessor complex mediates the genesis of microRNAs. *Nature* 432: 235–240. doi:10.1038/nature03120

Gruber AR, Martin G, Keller W, Zavolan M (2012) Cleavage factor Im is a key regulator of 3′ UTR length. *RNA Biol* 9: 1405–1412. doi:10.4161/rna.22570

Ha M, Kim VN (2014) Regulation of microRNA biogenesis. *Nat Rev Mol Cell Biol* 15: 509–524. doi:10.1038/nrm3838

He PY, Yip WK, Chai BL, Chai BY, Jabar MF, Dusa N, Mohtarrudin N, Seow HF (2017) Inhibition of cell migration and invasion by miR29a3p in a colorectal cancer cell line through suppression of CDC42BPA mRNA expression. *Oncol Rep* 38: 3554–3566. doi:10.3892/or.2017.6037

Hendrickson DG, Hogan DJ, Herschlag D, Ferrell JE, Brown PO (2008) Systematic identification of mRNAs recruited to argonaute 2 by specific microRNAs and corresponding changes in transcript abundance. *PLoS One* 3: e2126. doi:10.1371/journal.pone.0002126

Hendrickson DG, Hogan DJ, McCullough HL, Myers JW, Herschlag D, Ferrell JE, Brown PO (2009) Concordant regulation of translation and mRNA abundance for hundreds of targets of a human microRNA. *PLoS Biol* 7: e1000238. doi:10.1371/journal.pbio.1000238

Huppi K, Volfovsky N, Runfola T, Jones TL, Mackiewicz M, Martin SE, Mushinski JF, Stephens R, Caplen NJ (2008) The identification of microRNAs in a genomically unstable region of human chromosome 8q24. *Mol Cancer Res* 6: 212–221. doi:10.1158/1541-7786.MCR-07-0105

Ishikawa H, Yoshikawa H, Izumikawa K, Miura Y, Taoka M, Nobe Y, Yamauchi Y, Nakayama H, Simpson RJ, Isobe T, et al (2017) Poly(A)-specific ribonuclease regulates the processing of small-subunit rRNAs in human cells. *Nucleic Acids Res* 45: 3437–3447. doi:10.1093/nar/gkw1047

Jonas S, Izaurralde E (2015) Towards a molecular understanding of microRNA-mediated gene silencing. *Nat Rev Genet* 16: 421–433. doi:10.1038/nrg3965

Katoh T, Hojo H, Suzuki T (2015) Destabilization of microRNAs in human cells by 3′ deadenylation mediated by PARN and CUGBP1. *Nucleic Acids Res* 43: 7521–7534. doi:10.1093/nar/gkv669

Kertesz M, Iovino N, Unnerstall U, Gaul U, Segal E (2007) The role of site accessibility in microRNA target recognition. *Nat Genet* 39: 1278–1284. doi:10.1038/ng2135

Kim YK, Kim B, Kim VN (2016) Re-evaluation of the roles of DROSHA, export in 5, and DICER in microRNA biogenesis. *Proc Natl Acad Sci U S A* 113: E1881–E1889. doi:10.1073/pnas.1602532113

Kyritsis A, Papanastasi E, Kokkori I, Maragozidis P, Chatzileontiadou DSM, Pallaki P, Labrou M, Zarogiannis SG, Chrousos GP, Vlachakis D, et al (2022) Integrated deadenylase genetic association network and transcriptome analysis in thoracic carcinomas. *Molecules* 27: 3102. doi:10.3390/molecules27103102

Lai WS, Blackshear PJ (2001) Interactions of CCCH zinc finger proteins with mRNA: Tristetraprolin-mediated AU-rich element-dependent mRNA degradation can occur in the absence of a poly(A) tail. *J Biol Chem* 276: 23144–23154. doi:10.1074/jbc.M100680200

Lai WS, Kennington EA, Blackshear PJ (2003) Tristetraprolin and its family members can promote the cell-free deadenylation of AU-rich element-containing mRNAs by poly(A) ribonuclease. *Mol Cell Biol* 23: 3798–3812. doi:10.1128/MCB.23.11.3798-3812.2003

Lee JE, Lee JY, Trembly J, Wilusz J, Tian B, Wilusz CJ (2012) The PARN deadenylase targets a discrete set of mRNAs for decay and regulates cell motility in mouse myoblasts. *PLoS Genet* 8: e1002901. doi:10.1371/journal.pgen.1002901

Lee D, Park D, Park JH, Kim JH, Shin C (2019) Poly(A)-specific ribonuclease sculpts the 3′ ends of microRNAs. *RNA* 25: 388–405. doi:10.1261/rna.069633.118

Li S, Mei Z, Hu HB, Zhang X (2018) The lncRNA MALAT1 contributes to non-small cell lung cancer development via modulating miR-124/STAT3 axis. *J Cell Physiol* 233: 6679–6688. doi:10.1002/jcp.26325

Lin R, Maeda S, Liu C, Karin M, Edgington TS (2007a) A large noncoding RNA is a marker for murine hepatocellular carcinomas and a spectrum of human carcinomas. *Oncogene* 26: 851–858. doi:10.1038/sj.onc.1209846

Lin WJ, Duffy A, Chen CY (2007b) Localization of AU-rich element-containing mRNA in cytoplasmic granules containing exosome subunits. *J Biol Chem* 282: 19958–19968. doi:10.1074/jbc.M702281200

Mancini M, Grasso M, Muccillo L, Babbio F, Precazzini F, Castiglioni I, Zanetti V, Rizzo F, Pistore C, De Marino MG, et al (2021) DNMT3A epigenetically regulates key microRNAs involved in epithelial-to-mesenchymal transition in prostate cancer. *Carcinogenesis* 42: 1449–1460. doi:10.1093/carcin/bgab101

Maragozidis P, Karangeli M, Labrou M, Dimoulou G, Papaspyrou K, Salataj E, Pournaras S, Matsouka P, Gourgoulianis KI, Balatsos NA (2012) Alterations of deadenylase expression in acute leukemias: Evidence for poly(A)-specific ribonuclease as a potential biomarker. *Acta Haematol* 128: 39–46. doi:10.1159/000337418

Maragozidis P, Papanastasi E, Scutelnic D, Totomi A, Kokkori I, Zarogiannis SG, Kerenidi T, Gourgoulianis KI, Balatsos NA (2015) Poly(A)-specific ribonuclease and nocturnin in squamous cell lung cancer: Prognostic value and impact on gene expression. *Mol Cancer* 14: 187. doi:10.1186/s12943-015-0457-3

Martinez J, Ren YG, Nilsson P, Ehrenberg M, Virtanen A (2001) The mRNA cap structure stimulates rate of poly(A) removal and amplifies processivity of degradation. *J Biol Chem* 276: 27923–27929. doi:10.1074/jbc.M102270200

Mazzoccoli L, Robaina MC, Apa AG, Bonamino M, Pinto LW, Queiroga E, Bacchi CE, Klumb CE (2018) MiR-29 silencing modulates the expression of target genes related to proliferation, apoptosis and methylation in Burkitt lymphoma cells. *J Cancer Res Clin Oncol* 144: 483–497. doi:10.1007/s00432-017-2575-3

McKendrick L, Thompson E, Ferreira J, Morley SJ, Lewis JD (2001) Interaction of eukaryotic translation initiation factor 4G with the nuclear cap-binding complex provides a link between nuclear and cytoplasmic functions of the m(7) guanosine cap. *Mol Cell Biol* 21: 3632–3641. doi:10.1128/MCB.21.11.3632-3641.2001

Montellese C, Montel-Lehry N, Henras AK, Kutay U, Gleizes PE, O'Donohue MF (2017) Poly(A)-specific ribonuclease is a nuclear ribosome biogenesis factor involved in human 18S rRNA maturation. *Nucleic Acids Res* 45: 6822–6836. doi:10.1093/nar/gkx253

Moon DH, Segal M, Boyraz B, Guinan E, Hofmann I, Cahan P, Tai AK, Agarwal S (2015) Poly(A)-specific ribonuclease (PARN) mediates 3′-end maturation of the telomerase RNA component. *Nat Genet* 47: 1482–1488. doi:10.1038/ng.3423

Moraes KC, Wilusz CJ, Wilusz J (2006) CUG-BP binds to RNA substrates and recruits PARN deadenylase. *RNA* 12: 1084–1091. doi:10.1261/rna.59606

Mukherji S, Ebert MS, Zheng GXY, Tsang JS, Sharp PA, van Oudenaarden A (2011) MicroRNAs can generate thresholds in target gene expression. *Nat Genet* 43: 854–859. doi:10.1038/ng.905

Okamura K, Hagen JW, Duan H, Tyler DM, Lai EC (2007) The mirtron pathway generates microRNA-class regulatory RNAs in Drosophila. *Cell* 130: 89–100. doi:10.1016/j.cell.2007.06.028

Oulas A, Karathanasis N, Louloupi A, Iliopoulos I, Kalantidis K, Poirazi P (2012) A new microRNA target prediction tool identifies a novel interaction of a putative miRNA with CCND2. *RNA Biol* 9: 1196–1207. doi:10.4161/rna.21725

Qiu F, Sun R, Deng N, Guo T, Cao Y, Yu Y, Wang X, Zou B, Zhang S, Jing T, et al (2015) miR-29a/b enhances cell migration and invasion in nasopharyngeal carcinoma progression by regulating SPARC and COL3A1 gene expression. *PLoS One* 10: e0120969. doi:10.1371/journal.pone.0120969

Rachinger N, Fischer S, Böhme I, Linck-Paulus L, Kuphal S, Kappelmann-Fenzl M, Bosserhoff AK (2021) Loss of gene information: Discrepancies between RNA sequencing, cDNA microarray, and qRT-PCR. *Int J Mol Sci* 22: 9349. doi:10.3390/ijms22179349

Rehmsmeier M, Steffen P, Hochsmann M, Giegerich R (2004) Fast and effective prediction of microRNA/target duplexes. *RNA* 10: 1507–1517. doi:10.1261/rna.5248604

Ren YG, Martinez J, Virtanen A (2002) Identification of the active site of poly(A)-specific ribonuclease by site-directed mutagenesis and Fe(2+)-mediated cleavage. *J Biol Chem* 277: 5982–5987. doi:10.1074/jbc.M111515200

Ricci EP, Limousin T, Soto-Rifo R, Rubilar PS, Decimo D, Ohlmann T (2013) miRNA repression of translation in vitro takes place during 43S ribosomal scanning. *Nucleic Acids Res* 41: 586–598. doi:10.1093/nar/gks1076

Ruby JG, Jan CH, Bartel DP (2007) Intronic microRNA precursors that bypass Drosha processing. *Nature* 448: 83–86. doi:10.1038/nature05983

Rueden CT, Schindelin J, Hiner MC, DeZonia BE, Walter AE, Arena ET, Eliceiri KW (2017) ImageJ2: ImageJ for the next generation of scientific image data. *BMC Bioinformatics* 18: 529. doi:10.1186/s12859-017-1934-z

Ruegsegger U, Beyer K, Keller W (1996) Purification and characterization of human cleavage factor Im involved in the 3′ end processing of messenger RNA precursors. *J Biol Chem* 271: 6107–6113. doi:10.1074/jbc.271.11.6107

Salles FJ, Richards WG, Strickland S (1999) Assaying the polyadenylation state of mRNAs. *Methods* 17: 38–45. doi:10.1006/meth.1998.0705

Schmiedel JM, Klemm SL, Zheng Y, Sahay A, Blüthgen N, Marks DS, van Oudenaarden A (2015) Gene expression. MicroRNA control of protein expression noise. *Science* 348: 128–132. doi:10.1126/science.aaa1738

Seal R, Temperley R, Wilusz J, Lightowlers RN, Chrzanowska-Lightowlers ZM (2005) Serum-deprivation stimulates cap-binding by PARN at the expense of eIF4E, consistent with the observed decrease in mRNA stability. *Nucleic Acids Res* 33: 376–387. doi:10.1093/nar/gki169

Shevchenko A, Jensen ON, Podtelejnikov AV, Sagliocco F, Wilm M, Vorm O, Mortensen P, Shevchenko A, Boucherie H, Mann M (1996) Linking genome and proteome by mass spectrometry: Large-scale identification of yeast proteins from two dimensional gels. *Proc Natl Acad Sci U S A* 93: 14440–14445. doi:10.1073/pnas.93.25.14440

Shi Y, Manley JL (2015) The end of the message: Multiple protein-RNA interactions define the mRNA polyadenylation site. *Genes Dev* 29: 889–897. doi:10.1101/gad.261974.115

Shukla S, Schmidt JC, Goldfarb KC, Cech TR, Parker R (2016) Inhibition of telomerase RNA decay rescues telomerase deficiency caused by dyskerin or PARN defects. *Nat Struct Mol Biol* 23: 286–292. doi:10.1038/nsmb.3184

Shukla S, Bjerke GA, Muhlrad D, Yi R, Parker R (2019) The RNase PARN controls the levels of specific miRNAs that contribute to p53 regulation. *Mol Cell* 73: 1204–1216 e4. doi:10.1016/j.molcel.2019.01.010

Stuart BD, Choi J, Zaidi S, Xing C, Holohan B, Chen R, Choi M, Dharwadkar P, Torres F, Girod CE, et al (2015) Exome sequencing links mutations in PARN and RTEL1 with familial pulmonary fibrosis and telomere shortening. *Nat Genet* 47: 512–517. doi:10.1038/ng.3278

Suswam E, Li Y, Zhang X, Gillespie GY, Li X, Shacka JJ, Lu L, Zheng L, King PH (2008) Tristetraprolin down-regulates interleukin-8 and vascular endothelial growth factor in malignant glioma cells. *Cancer Res* 68: 674–682. doi:10.1158/0008-5472.CAN-07-2751

Talbot LJ, Bhattacharya SD, Kuo PC (2012) Epithelial-mesenchymal transition, the tumor microenvironment, and metastatic behavior of epithelial malignancies. *Int J Biochem Mol Biol* 3: 117–136.

Tamaddon M, Shokri G, Hosseini Rad SMA, Rad I, Emami Razavi A, Kouhkan F (2020) Involved microRNAs in alternative polyadenylation intervene in breast cancer via regulation of cleavage factor "CFIm25". *Sci Rep* 10: 11608. doi:10.1038/s41598-020-68406-3

Tang W, Tu S, Lee HC, Weng Z, Mello CC (2016) The RNase PARN-1 trims piRNA 3′ ends to promote transcriptome surveillance in C. elegans. *Cell* 164: 974–984. doi:10.1016/j.cell.2016.02.008

Tran H, Maurer F, Nagamine Y (2003) Stabilization of urokinase and urokinase receptor mRNAs by HuR is linked to its cytoplasmic accumulation induced by activated mitogen-activated protein kinase-activated protein kinase 2. *Mol Cell Biol* 23: 7177–7188. doi:10.1128/MCB.23.20.7177-7188.2003

Tummala H, Walne A, Collopy L, Cardoso S, de la Fuente J, Lawson S, Powell J, Cooper N, Foster A, Mohammed S, et al (2015) Poly(A)-specific ribonuclease deficiency impacts telomere biology and causes dyskeratosis congenita. *J Clin Invest* 125: 2151–2160. doi:10.1172/JCI78963

Wu L, Fan J, Belasco JG (2006) MicroRNAs direct rapid deadenylation of target mRNAs. *Proc Natl Acad Sci U S A* 103: 4034–4039. doi:10.1073/pnas.0510928103

Xiao Z, Wang Y, Ding H (2019) XPD suppresses cell proliferation and migration via miR-29a3p-Mdm2/PDGF-B axis in HCC. *Cell Biosci* 9: 6. doi:10.1186/s13578-018-0269-4

Yoda M, Cifuentes D, Izumi N, Sakaguchi Y, Suzuki T, Giraldez AJ, Tomari Y (2013) Poly(A)-specific ribonuclease mediates 3′-end trimming of Argonaute2-cleaved precursor microRNAs. *Cell Rep* 5: 715–726. doi:10.1016/j.celrep.2013.09.029

Zhang X, Devany E, Murphy MR, Glazman G, Persaud M, Kleiman FE (2015) PARN deadenylase is involved in miRNA-dependent degradation of TP53 mRNA in mammalian cells. *Nucleic Acids Res* 43: 10925–10938. doi:10.1093/nar/gkv959

Mutual feedback regulation between Poly(A)-specific ribonuclease (PARN) and cognate microRNAs

Athanasios Kyritsis, Rafailia AA Beta, Diana Scutelnic, Vasiliki Stravokefalou, Valerio Del Vescovo, Zoi V Arsenopoulou, Konstantinos Papikinos, Margherita Grasso, Francesca Fontana, Paraskevi Moutopoulou, Alexandros Tsiporis, Martina Samiotaki, George Panayotou, Michela A DentiNikolaos AA Balatsos

Vol 9 | No 5 | e202503341
http://doi.org/10.26508/lsa.202503341